EUROPEAN ORGANIZATION FOR NUCLEAR RESEARCH
ORGANISATION EUROPEENNE POUR LA RECHERCHE NUCLEAIRE

CERN - PS DIVISION

PS / DI / Note 99-20
AD Note053

SIMULATIONS OF ELECTRON COOLING USING 'BETACOOL'

N. Madsen

Geneva, Switzerland
September 23, 1999

Contents

Introduction

Electron cooling is important for the success of the Anti-proton Decelerator (AD) [1]. The reason for this, discussed in reference [2], is that multiple scattering on the residual-gas becomes dominant in the anti-proton beam at the low final energies to be attained in the AD, and that the beam blows up adiabatically during deceleration. Multiple scattering causes emittance increase of the beam, which, without cooling, would cause the beam lifetime to be too short. Furthermore the experiments to be conducted with the anti protons set upper limits to the acceptable emittances, which are by far lower than what can be expected without cooling [3, 4].

This report is a summary of work done in order to investigate the feasibility of the program BETACOOL [5] as a way of predicting cooling times. This program simulates electron cooling of single particles in a storage ring. It does not include collective effects in the particle beam to be cooled, however, it includes dispersion effects, as well as lattice effects at the electron cooler, and also space-charge and magnetic effects in the electron beam. In order to determine the usefulness of the program, multiple simulation runs have been carried out and compared to measurements done in LEAR [6]. The objective is to scale from the LEAR results to the situation in the AD.

The report is split into 5 chapters. The first chapter discusses an analytical approach to the physics of electron cooling. Several important aspects for the cooling process are discussed and order of magnitude estimates are made in order to get a feeling for the behaviour to be expected in the experiments as well as the simulations. The second chapter reviews some electron-cooling experiments done at LEAR, which in the third chapter are compared to simulations in order to establish how to use the simulation program, and how well experimental data can be reproduced in simulations. In the fourth chapter the simulation program is used to predict cooling times in the AD. The last chapter summarizes the results and draws some conclusions.

Chapter I

Theoretical Discussion

In this chapter we review some of the existing analytical electron-cooling theory. The discussion is based on Ref. [7]. Furthermore we discuss, analytically, a range of other aspects which influence the cooling. This covers space-charge induced dispersion in the electron beam, dispersion in the ring lattice, $E \times B$ drift, and betatron motion. The purpose of this study, which due to the complexity and large number of the processes cannot be completely covered analytically is to gain some insight in which processes we may expect to be important under various circumstances, in order to better evaluate the results from various cooling experiments as well as the outcome of the simulations.

1.1 Simple expressions for friction and diffusion

As is well known, and described in some detail in [7], electron cooling relies on mixing a cold gas of electrons with the relatively hot beam. The mean velocity of the electron beam is matched to the mean velocity of the ion beam and thus in the rest frame of the particles we have a mixture of two gases of different temperature, and via the Coulomb interactions of the particles the system will equilibrate. However, if we continuously replace the electrons with cold electrons we can eventually cool the ions to the same temperature as the electrons.

Once embedded in the cold electron cloud the circulating ion beam will experience a friction force as well as multiple scattering on the electrons (diffusion). A good review of this is given in [7]. Here we shall briefly summarize the results.

1.1.1 Friction of the electron beam

We are mainly interested in the change in the emittance of the beam, and thus the transverse development. The transverse friction force on the circulating ions from the electron beam is

$$F_\perp = -v_{p,\perp} 4\pi\eta n_e Z^2 r_e^2 m_e c^4 L_C \times \begin{cases} \frac{1}{v_p^3} & ; \quad v_p > \Delta_\perp \\ \frac{1}{\Delta_\perp^3} & ; \quad \Delta_{||} < v_p < \Delta_\perp \\ 0 & ; \quad v_p < \Delta_{||} \end{cases} \tag{1.1}$$

where $\Delta_{\perp,||}$ is the RMS electron thermal velocity in the rest frame of the particles., m is the electron mass, n_e is the electron density in the center of mass frame of reference, L_C is the Coulomb logarithm, $\mathbf{v_p}$ is the rest frame RMS thermal velocity of the circulating particles, η is the fraction of the ring occupied by the electron cooler (sometimes one incorporates this factor in the electron density and use the effective electron density instead), and $r_e = e^2/4\pi\epsilon_0 mc^2$ is the classical electron radius. The longitudinal electron temperature is much smaller than the transverse, due to the acceleration in the electron cooler. At super low anti-proton temperatures, the transverse component of the friction force vanishes.

The Coulomb logarithm L_C stems from the integral over all angles in the Rutherford cross section. When the scattering angles are very small, it is equivalent to large impact parameters, and we can no longer assume that we have a binary collision, as the other particles in the gas contributes with a shielding factor expressed by the Debye length. On the other hand the maximum angle possible or rather the minimum impact parameter is given by the maximum energy transfer possible which in turn in given by the relative velocity of the colliding particles.

The Coulomb logarithm is given by [7]

$$L_C = \ln\left(\frac{b_{max}}{b_{min}}\right) \tag{1.2}$$

where b_{min} and b_{max} are the minimum and maximum impact parameters. The usual minimum impact parameter assumed is

$$b_{min} = \frac{e^2}{4\pi\epsilon_0 m_e(v_p^2 + \Delta_\perp^2)} = r_e\left(\frac{c^2}{v_p^2 + \Delta_\perp^2}\right) \tag{1.3}$$

where $r_e = e^2/4\pi\epsilon_0 m_e c^2$ is the classical electron radius. The maximum impact parameter is the Debye screening length unless the electron beam is smaller. The Debye length is given by

$$\lambda_D = \frac{\sqrt{\langle \mathbf{U}^2 \rangle}}{\omega_{pe}} \sim \sqrt{\Delta_\perp^2 + v_p^2} \cdot \sqrt{\frac{m_e\epsilon_0}{n_e e^2}} \tag{1.4}$$

where U is the relative velocity of the particle and the electron colliding with it in the electron frame, and $\omega_{pe} = \sqrt{4\pi n_e r_e c^2}$ is the electron plasma frequency.

1.1.2 The cooling time

Neglecting betatron oscillations (for now) the e-folding cooling time (in the center-of-mass frame) can be calculated from the friction force as (assuming linear dependence in v, which is true for small v)

$$\tau_\perp = -\left(\frac{1}{m_p}\left.\frac{dF_\perp(v_p)}{dv_p}\right|_{v_p=0}\right)^{-1} \tag{1.5}$$

which with equation (1.1) can be written

$$\tau_\perp = \frac{1}{4\pi\eta n_e Z^2 r_e r_p c^4 L_C} \times \begin{cases} \Delta_\perp^3 & ; \ \Delta_{||} < v_p < \Delta_\perp \\ \infty & ; \ v_p < \Delta_{||} \end{cases} \tag{1.6}$$

Equation (1.6) only makes sense when the friction force is not divergent in zero (as it is for $v_p > \Delta_\perp$).

To get the cooling time in the laboratory frame, we need to take the time dilation as well as Lorentz contraction into consideration. After conversion to more practical parameters we find that the electron density is given by [7]

$$n_e = \frac{I_e}{e\gamma\beta c\pi a^2} \tag{1.7}$$

where a is the cross section radius of the electron beam, I_e the electron current in the lab-frame, and γ and β the relativistic factors of the electron beam.

In the laboratory frame the cooling time is then given by

$$\tau_\perp^{lab} = \frac{a^2 e\gamma^2\beta}{4\eta I_e Z^2 r_e r_p c^3 L_C} \times \begin{cases} \Delta_\perp^3 & ; \ \Delta_{||} < v_p < \Delta_\perp \\ \infty & ; \ v_p < \Delta_{||} \end{cases} \tag{1.8}$$

1.1.3 Diffusion

Apart from friction the multiple scattering on the electrons also introduce a diffusion in the circulating particle beam, which however under most circumstances will be weaker than the heating due to intra-beam scattering and scattering on the rest gas.

The diffusion coefficient due to multiple scattering on electrons is given by [7][1]

$$D = 4\pi\eta n_e Z^2 r_p^2 c^4 L_C \times \begin{cases} 1/v_p & ; \ v_p > \Delta_\perp \\ 1/\Delta_\perp & ; \ v_p < \Delta_\perp \end{cases} \tag{1.9}$$

where m_p is the mass of the circulating particles, L_C is the Coulomb logarithm, and $r_p = e^2/4\pi\epsilon_0 m_p c^2$ is the classical proton radius.

Another thing which we may be interested in is how the electron beam is influenced by the circulating particles. This may become important in long electron coolers, or electron coolers which recycle the electron beam more times. The diffusion in the electron beam can be found easily by 'inverting' the above equation

$$D_e = 4\pi n_p r_e^2 c^4 L_C \times \begin{cases} 1/v_p & ; \ v_p > \Delta_\perp \\ 1/\Delta_\perp & ; \ v_p < \Delta_\perp \end{cases} \tag{1.10}$$

where n_p is the local density of the circulating particles.

A calculation of the relative change in the transverse thermal energy of the electron beam (which is initially 0.1 eV) for various machine settings is listed in Table 1.1. The calculations have assumed that the thermal velocity spread develops as

$$\sigma = \sigma_0 + \sqrt{2D_e t} \tag{1.11}$$

where t is the time.

[1] Notice that there is a misprint in the $Q_\perp$ equation in (1.28) in [7]. The mass stated should have been M and not m.

Machine	$\Delta\sigma/\sigma_0$(1.5m)	$\Delta\sigma/\sigma_0$(3.0m)
LEAR, 96-1, Pb. beam at 4.2 MeV/nucl.	$4.7{\cdot}10^{-4}$	$6.6{\cdot}10^{-4}$
LEAR, 96-1, Protons at 310 MeV/c	$2.7{\cdot}10^{-4}$	$3.7{\cdot}10^{-4}$
AD, (Anti)protons at 300 MeV/c	$2.8{\cdot}10^{-4}$	$4.0{\cdot}10^{-4}$
AD, (Anti)protons at 100 MeV/c	$1.0{\cdot}10^{-3}$	$1.5{\cdot}10^{-3}$

Table 1.1: Calculations of the relative change of the transverse thermal velocity of the cooling electron beam after passage though some distance of the circulating ions in the cooler.

The calculations listed in Table 1.1 shows that we do not need to worry about this effect in the present experiments, as it is negligible.

Another effect which could be important is the intra-beam scattering in the electron beam itself. This effect can be estimated using the results in Ref. [2]. The transverse degree of freedom of the electron beam is cooled slowly by the cold longitudinal, and the effect is slow compared to the time it takes for an electron to traverse the cooler. The longitudinal diffusion on the other hand results in a growth time of about 10% of the passage time in the case with the highest electron density (LEAR, 96-1 Pb at 4.2 MeV/nucl.). As the longitudinal temperature is extremely low and the longitudinal cooling time is therefore very fast compared to the transverse, we do not expect much influence from IBS in the electron beam. This has been confirmed by a series of simulations using the procedures of chapter 3 in which the longitudinal electron temperature was varied an order of magnitude without noticeable effects on the transverse cooling time.

1.1.4 The longitudinal magnetic field

A thing which we have ignored in the above calculations is the longitudinal magnetic field introduced in the cooling section by a solenoid. This can be included in the friction calculation, but we can also make some simple estimates on how much we would expect this field to influence both the electrons, and thus the friction, but also the circulating beam and thereby introduce a coupling between horizontal and vertical betatron motion.

The cyclotron frequency of a particle with charge number z moving perpendicular to a magnetic field is

$$\omega_c = \frac{zeB}{\gamma mc} \tag{1.12}$$

and the radius of the cyclotron motion is

$$r_c = \frac{mv}{zeB} \tag{1.13}$$

In order to evaluate the expected influence of this motion we can calculate the cyclotron tune, which is the number of cyclotron periods during the passage through the electron cooler,

$$Q_c = \frac{\omega_c}{2\pi}\frac{v_0}{L_{ecool}} \tag{1.14}$$

Table 1.2 lists some radii and tunes for various machine settings discussed in this note.

Machine	r_c (e^-)	$Q_{c,elec.}$	$Q_{c,beam}$
LEAR, 96-1, Pb. beam at 4.2 MeV/nucl.	$4.6 \cdot 10^{-8}$ m	$4.0 \cdot 10^{4}$	$1.9 \cdot 10^{-3}$
LEAR, 96-1, Protons at 310 MeV/c	$2.5 \cdot 10^{-6}$ m	$2.2 \cdot 10^{2}$	$1.2 \cdot 10^{-1}$
AD, (Anti)protons at 300 MeV/c	$2.1 \cdot 10^{-5}$ m	$2.3 \cdot 10^{1}$	$1.3 \cdot 10^{-2}$
AD, (Anti)protons at 100 MeV/c	$2.1 \cdot 10^{-5}$ m	$6.6 \cdot 10^{1}$	$3.6 \cdot 10^{-2}$

Table 1.2: Calculation of the influence of a longitudinal magnetic field of 500 Gauss in the cooling section on the electron motion and the ion beam motion.

These results show that we may introduce a large coupling between the two transverse dimensions with the present setup - keep in mind that a cyclotron tune for the beam of 0.25 ($Q_{c,beam}$) completely interchanges the horizontal motion and vertical motion in one passage of the cooler. The influence of the solenoid on the circulating beam was however compensated in the experiments discussed in this note.

The results for the electron beam indicates that this is an effect which is important, as the small radii indicates that the electrons are transversely well localized in the beam (which has a total radius of 2.5 cm). When the magnetic field is strong enough that the electrons in practice does not have any transverse motion, the electron beam is said to be magnetized. The field at which the magnetic influence becomes significant can be estimated by [7]

$$B \geq \frac{800}{z^{1/3}} G \tag{1.15}$$

which is fulfilled for the lead ions in LEAR, and almost fulfilled for the other situations. In a magnetized electron beam the friction equation changes, and becomes considerably more complicated, but one main feature which appears, is that the important velocity in the friction equation becomes the *longitudinal* instead of the *transverse* electron velocity.

However, as we will see in the simulations (which include these effects) it is hard to put up a general analytical expression for magnetized cooling which gives good insight. We will therefore refrain from going into more detail at this point, and instead look at a few other important aspects, were analytical studies will give us some insight.

1.2 Dispersion in the electron beam

Before investigating the various results from measurements and simulations it is worth introducing one concept which is important to the efficiency of electron cooling, when a large cooling force is desired.

1.2.1 Space-charge in the electron beam

Increasing the electron density will increase the cooling rate, however when the density becomes high enough that the Coulomb force between the electrons becomes important the velocity spread of the electron beam becomes perturbed.

If we assume that we have a spatially uniform axisymmetric beam of electrons, the transverse electric field from the beam can, via Gauss law be found to be

$$E_\perp(r) = \frac{\lambda}{2\pi\epsilon_0} \begin{cases} \frac{r}{a^2} & ; \ 0 \le r \le a \\ \frac{1}{r} & ; \ a \le r \le b \end{cases} \tag{1.16}$$

where λ is the longitudinal charge density in the rest frame. This can be expressed via the electron current as $\lambda = I_e/v_e$, where v_e is the electron velocity. The resulting potential across the electron beam if we assume that the beam is surrounded by a grounded vacuum chamber of radius b can the be found to be

$$\begin{aligned} \Phi_{sc}(r) &= -\int_b^r E_\perp(r)\, dr \\ &= \frac{\lambda}{4\pi\epsilon_0}\left[2\ln\frac{a}{b} - \frac{r^2}{a^2} + 1\right] \ ; \ 0 < r < a \end{aligned} \tag{1.17}$$

or in terms of the electron current

$$\Phi_{sc}(r) = \frac{I_e}{4\pi\epsilon_0\beta\cdot c}\left[2\ln\frac{b}{a} + \frac{r^2}{a^2} - 1\right] \ ; \ 0 < r < a \tag{1.18}$$

If the beam is accelerated across a potential difference of $\Phi_0 \gg \Phi_{sc}(r)$ then the kinetic energy gain of the electron beam will be

$$E_k(r) = \Phi_0 + \Phi_{sc}(r) \tag{1.19}$$

thus the velocity of a given electron (starting at rest) will be

$$v(r) = c\sqrt{1 - \left(\frac{mc^2}{E_k(r) + mc^2}\right)^2} \underset{\approx}{\text{non-rel}} \sqrt{\frac{2E_k(r)}{m}} \tag{1.20}$$

the variation in acceleration potential results in the following variation in velocity across the electron beam (with respect to the velocity of the electrons on axis)

$$\begin{aligned} \frac{\Delta v}{v}(r) &= \frac{v(r) - v(0)}{v(0)} \\ &\underset{\approx}{\text{non-rel}} \frac{\sqrt{\Phi_0 + \Phi_{sc}(r)} - \sqrt{\Phi_0 + \Phi_{sc}(0)}}{\sqrt{\Phi_0 + \Phi_{sc}(0)}} \\ &\approx \frac{1}{2}\frac{\Phi_{sc}(r) - \Phi_{sc}(0)}{\Phi_0} \end{aligned} \tag{1.21}$$

which can be written explicitly as

$$\frac{\Delta v}{v}(r) = r^2 \frac{I_e}{8\pi\epsilon_0\beta\cdot c\cdot a^2\Phi_0} \tag{1.22}$$

Machine	I_e	$\Delta v/v$	E_{sc}
LEAR, 96-1, Pb. beam at 4.2 MeV/nucl.	0.3 A	$2.1 \cdot 10^{-2}$	$2.0 \cdot 10^{-1}$ eV
LEAR, 96-1, Protons at 310 MeV/c	1.0 A	$1.7 \cdot 10^{-3}$	$1.5 \cdot 10^{-2}$ eV
AD, (Anti)protons at 300 MeV/c	2.5 A	$4.8 \cdot 10^{-3}$	$1.1 \cdot 10^{-1}$ eV
AD, (Anti)protons at 100 MeV/c	0.3 A	$1.5 \cdot 10^{-2}$	$1.2 \cdot 10^{-1}$ eV

Table 1.3: Calculations of the relative velocity offset of electrons at the edge of the electron beam compared to the electrons in the center. The equivalent pseudo temperatures (in eV) are also shown.

Table 1.3 lists some examples of the relative velocity offset of the electrons at the edge of the electron beam from the electrons in the center in various cases discussed in this note.

When electron cooling protons (with the energy and the electron currents used in the experiments discussed here) the influence of space-charge is smaller for lead ions, as the acceleration of the electrons is larger. If an ion beam is cooled by a dispersive electron beam and the lattice dispersion is zero in the cooler, we may assume that the final RMS velocity spread of the ion beam will reflect the RMS velocity spread of the electron beam (this situation is thus usually present in the vertical dimension).

The electron beam has a radius a, and the RMS velocity spread of the space-charge distorted electron beam can found to be given by

$$\langle v^2 \rangle = \frac{1}{5} \left[\frac{\Delta v}{v} (a)\, v(0) \right]^2 \tag{1.23}$$

where the factor of $1/5$ stems from the parabolic shape of the velocity distribution [8].

From equation (1.23) we can define a temperature as

$$T = \frac{m}{k_B} \langle v^2 \rangle = \frac{m}{5k_B} \left[\frac{\Delta v}{v} (a)\, v(0) \right]^2 \tag{1.24}$$

If a beam is cooled in a section without dispersion for the circulating particles, this space-charge induced velocity spread and longitudinal temperature of the electron beam can be used to estimate the final longitudinal velocity distribution of the circulating ions. As long as this 'virtual' temperature is much smaller than the transverse temperature of the electron beam this will not change the cooling times. In order to compare the space-charge induced velocity spread with the electron beam temperature, which is normally given as the RMS kinetic energy, we can use the following equation

$$E_{sc,ebeam} = \frac{1}{2} m \langle v^2 \rangle = \frac{1}{10} m \left[\frac{\Delta v}{v} (a)\, v(0) \right]^2 \tag{1.25}$$

in Table 1.3 we have shown some pseudo temperatures for typical machine settings. The typical transverse electron temperature is about 0.1 eV (the longitudinal is much smaller) thus, as we can see from the table, space-charge may introduce longitudinal velocity spreads comparable to the transverse temperature, and may therefore influence the cooling time considerably.

1.2.2 Dispersion in the stored beam

If the section with the cooling is dispersive, which from the results of the experiments seems to be beneficial for the cooling, the calculation becomes more complicated. The closed orbit dispersion is to first order given by

$$\Delta x = D_h \frac{\Delta p}{p} = D_h \gamma^2 \frac{\Delta v}{v} \tag{1.26}$$

where D_h is the dispersion function of the storage ring in the cooling section. Thus the longitudinal velocity of the circulating ions varies linearly as a function of horizontal closed orbit position.

Now, when the ion and electron beams are merged the interaction will cause an ion to be accelerated/decelerated to the same velocity as the electron beam at its position. As the electron beam also exhibits dispersion, the cooling time will depend on the vertical distance between the electron dispersion parabola and the ion dispersion line at the position x, i.e. on the ions longitudinal velocity. As the ions exhibit betatron oscillations it will also depend on the emittance.

If we consider ions without betatron oscillations, we observe that when the initial longitudinal velocity of the ion beam is such that $(v_{\|} - v_e(\Delta x)) < 0$, where $\Delta x > 0$ is the position deviation of an ion with velocity $v_{\|}$, then the ion beam will be accelerated by the electron beam, and due to dispersion Δx will increase further, and as v_e grows quadratically with position the situation is unstable. This 'heating' mechanism which is present for $\Delta x > \Delta x_0$ is illustrated in Figure 1.1.

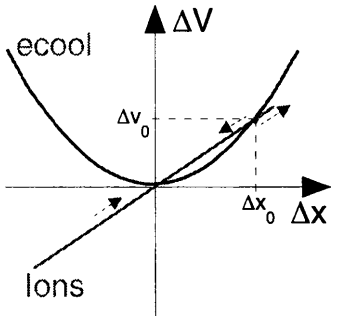

Figure 1.1: Dispersion in electron beam and ion beam. The arrows shows which direction the interaction will accelerate the ion beam constituents.

With betatron oscillations it is necessary to average between the periods of cooling and the periods of heating in order to estimate when the beam is heated. The cross over point between heating and cooling can be easily found using the results above.

$$\Delta x_0 = \frac{8\pi\epsilon_0\beta c a^2 \Phi_0}{I_e D_h \gamma^2} \tag{1.27}$$

where the betatron oscillations have been ignored. In table 1.4 are shown some examples of cross over points (and the corresponding momentum offsets) calculated using setups discussed in this note.

Machine	I_e	D_h	Δx_0	$\Delta p/p$
LEAR, 96-1, Pb. beam at 4.2 MeV/nucl.	0.3 A	3.6 m	0.0082 m	0.0023
LEAR, 96-1, Protons at 310 MeV/c	1.0 A	3.6 m	0.089 m	0.025
AD, (Anti)protons at 300 MeV/c	2.5 A	0.144 m	0.82 m	5.6
AD, (Anti)protons at 100 MeV/c	0.3 A	0.144 m	0.29 m	2.0

Table 1.4: Cross over points for various machines described throughout this note. Note that in the AD the dispersion is only 0.144 m in the electron cooler.

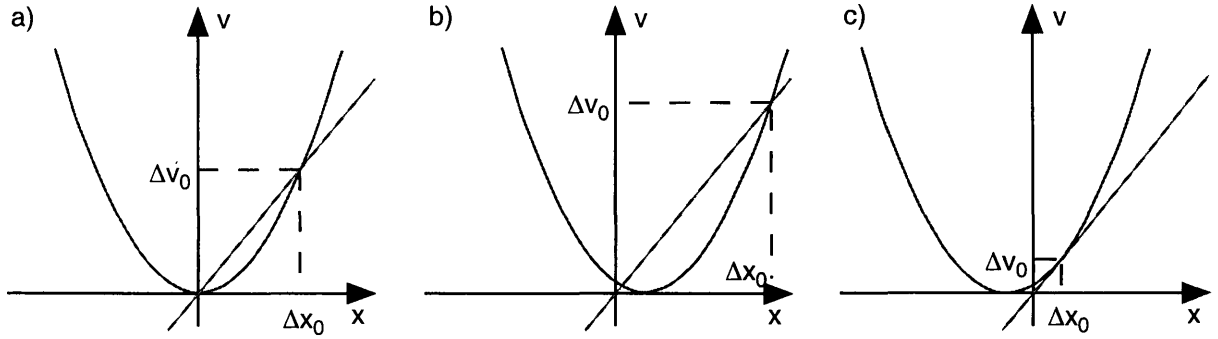

Figure 1.2: Longitudinal velocity versus horizontal position. The parabola illustrates the velocity distribution in the electron beam. The straight line illustrates the dispersion in the ion beam. a) Electron and ion beam are aligned. b) Electron beam is moved outwards (positive) with respect to the ions. c) Electron beam is moved inwards.

In the experiments we have the possibility of displacing the electron and ion beam with respect to each other. In figure 1.2 we have illustrated how this changes the cooling force.

Figure 1.2 shows that when the electron beam is moved in the positive x-direction, we still have a cooling until the cross over point which is moved outwards (positive direction). Ultimately this will lead to worse cooling as the velocity difference between the ions and the electrons increases and the overlap of the electron with the ions will also decrease. If we instead move the electron beam in the negative x-direction (inwards) the cut-off momentum offset decreases, and we may end with a situation with no cooling. We can calculate the position at which negative displacement of the electron beam causes loss of cooling. This is the position where the ion beam dispersion line in Figure 1.2 crosses the electron beam velocity profile only once.

$$\Delta x^e_{cut} = -\frac{1}{4}\Delta x_0 \tag{1.28}$$

1.3 E×B drift due to space-charge

As mentioned in the last part of section 1.1 a longitudinal magnetic field is introduced in the electron beam, mainly for reasons of stability and guidance of the electron beam, but in recent years also in order to decrease the electron transverse temperature via adiabatic expansion (a

stronger magnetic field is introduced in the electron gun, and due to adiabatic conservation the magnetic moment [9], the transverse electron velocity decreases).

The longitudinal magnetic field together with the transverse electromagnetic forces due to space-charge induces a cyclic drift motion, know as E×B drift, as the force on a particle is :

$$\mathbf{F} = q\mathbf{E}_{sc} + q\mathbf{v} \times (\mathbf{B}_{sol} + \mathbf{B}_{sc}) \tag{1.29}$$

which in our case gives an cyclic motion with a moving center, with a velocity of magnitude

$$v_d = \frac{E_{sc}}{B_{sol}\gamma^2} \tag{1.30}$$

which add (in square) to the transverse thermal velocity of the electrons (to first order).

Inserting the space-charge field from equation (1.16)

$$v_d(r) = \frac{\lambda}{2\pi\epsilon_0 B_{sol}\gamma^2}\frac{r}{a^2} \; ; \; 0 \leq r \leq a \tag{1.31}$$

which for comparison we have calculated at the edge of the electron beam for our 4 standard setups in Table 1.5.

Machine	I_e	$v_d(a)$ [m/s]	$v_d(a)/\Delta_\perp$	$v_d(\epsilon_{init})/\Delta_\perp$
LEAR, 96-1, Pb. beam at 4.2 MeV/nucl.	0.3 A	$1.3{\cdot}10^5$	0.6	0.3
LEAR, 96-1, Protons at 310 MeV/c	1.0 A	$1.5{\cdot}10^5$	0.07	0.03
AD, (Anti)protons at 300 MeV/c	2.5 A	$3.3{\cdot}10^5$	1.8	1.4
AD, (Anti)protons at 100 MeV/c	0.3 A	$1.1{\cdot}10^5$	0.6	0.2

Table 1.5: Velocity of $E \times B$ drift at the edge of the electron beam for a typical magnetic field of 0.06 Tesla. The table also lists the ratio of this velocity to the transverse thermal electron velocity, as well as the ratio with the drift velocity at the edge of a typical initial ion beam (ϵ_h = 40 π and ϵ_v = 10 π).

Table 1.5 lists both the drift velocities at the edge of the electron beam as well as their relation to the transverse thermal velocity of the electrons. As the velocities add in square the change in the effective thermal velocity is weak in the drift velocity, thus equal velocities correspond to an 40% increase in the effective velocity. We do however observe from the table that for the AD with a 300 MeV/c beam the influence of the $E \times B$ drift may be large.

1.4 Betatron Motion

So far we have ignored the betatron motion of the particles in our considerations. This first of all alters the cooling time, as we need to consider the system as a damped oscillator. This is discussed in detail in reference [7]. The resulting cooling time, including friction is twice the cooling time given by equation 1.8, i.e.

$$\tau^{lab}_{\perp,\beta} = \frac{a^2 e\gamma^2\beta}{2\eta I_e Z^2 r_e r_p c^3 L_C} \times \begin{cases} \Delta_\perp^3 & ; \; \Delta_{||} < v_p < \Delta_\perp \\ \infty & ; \; v_p < \Delta_{||} \end{cases} \tag{1.32}$$

1.4.1 Horizontal Betatron Oscillations

The betatron motion will also change the influence of the electron beam dispersion, as the oscillations will bring particles into areas of force with varying sign. A few different situations have been shown in Figure 1.3.

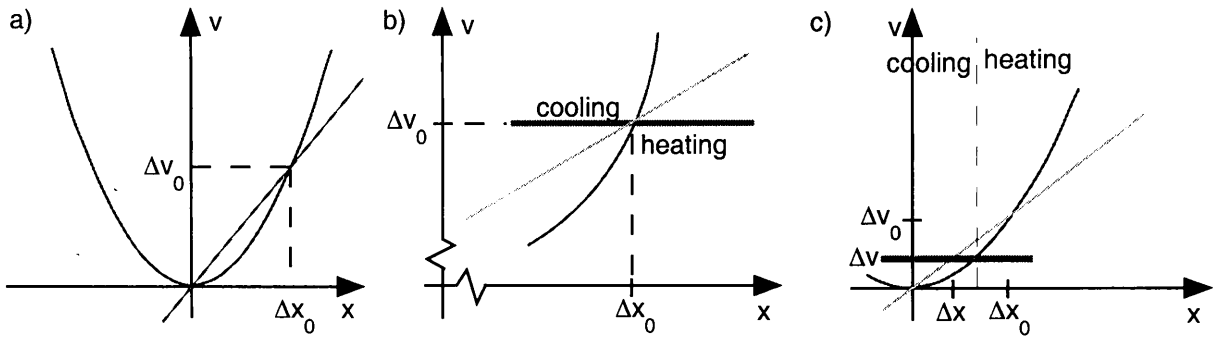

Figure 1.3: The change of the force on a particle during its horizontal betatron motion. See discussion in the text.

Figure 1.3.a shows the situation as viewed so far. The cross over point at Δx_0 is the point at which a higher momentum off set of the particle to be cooled will result in heating. Figure 1.3.b shows a blowup of the region around the cross over point. The thick horizontal line illustrates the horizontal betatron motion of a particle with a velocity offset corresponding to Δv_0. Assuming the friction force scales linearly with the velocity difference between the electron beam and the ion in question, we find that with betatron motion the particle will be heated at Δx_0, thus the cross over point with betatron motion is at a lower Δv than without betatron motion. In figure 1.3.c the particle velocity offset is $\Delta v' < \Delta v_0$, and we see that we may have an average force which is cooling. If on the other hand the force is inversely proportional to velocity, we may find that the cross over point increases with emittance (amplitude of betatron motion).

We see from the discussion above that we have to average over the force during a betatron oscillation, as it is the average force on the particle which determines whether it will be cooled or heated. In order to calculate the average friction force we need the velocity offset of an ion to the electron beam as a function of betatron phase (position). We earlier found the relative velocity offset in the electron beam to be given by equation (1.22). Thus for a particle with longitudinal velocity offset $\Delta v_{\|}$ to the mean beam velocity v_0, and horizontal emittance ϵ_h the velocity offset from the electron beam in terms of horizontal betatron phase ϕ is given by

$$\Delta v_{\|}^{\beta}(\phi) = \Delta v_{\|} - v_0 \cdot \frac{\Delta v}{v}\left(D_h \gamma^2 \frac{\Delta v_{\|}}{v_0} + \sqrt{\epsilon_h \beta_h}\sin\phi\right) \tag{1.33}$$

thus the average longitudinal friction force is given by

$$F_{\|}^{\beta}(\Delta v_{\|}, \epsilon_h) = \frac{1}{2\pi}\int_0^{2\pi} F_{\|}(\Delta v_{\|}^{\beta}(\phi))d\phi \tag{1.34}$$

where the longitudinal friction force is given by [7]

$$F_{\parallel}(v_{p,\parallel}) = -v_{p,\parallel} 4\pi\eta n_e Z^2 r_e^2 m_e c^4 L_C \times \begin{cases} \frac{1}{v_p^3} & ; \ v_p > \Delta_\perp \\ \frac{1}{v_{p,\parallel}\Delta_\perp^2} & ; \ \Delta_{\parallel} < v_p < \Delta_\perp \\ \frac{1}{\Delta_{\parallel}\Delta_\perp^2} & ; \ v_p < \Delta_{\parallel} \end{cases} \tag{1.35}$$

In order to get at simple expression we may assume that the friction force is linear, and we find that the average friction is given by

$$F_{\parallel}^{\beta}(v_{p,\parallel}) = -\frac{4\pi\eta n_e Z^2 r_e^2 m_e c^4 L_C}{v_p^3}\left[v_{p,\parallel} - \frac{I_e v_0}{8\pi\epsilon_0\beta c a^2 \Phi_0}\left(D_h^2\gamma^4\frac{v_{p,\parallel}^2}{v_0^2} + \frac{1}{2}\epsilon_h\beta_h\right)\right] \tag{1.36}$$

from which we can calculate the betatron modified cross over point, by using that $F_{\parallel}^{\beta} = 0$ and $dF_{\parallel}^{\beta}/dv > 0$ at the cross over point.

$$\Delta v_0^{\beta} = \frac{1}{2}\Delta v_0 + \frac{1}{2}\Delta v_0\sqrt{1 - \frac{2\epsilon_h\beta_h}{D_h^2\gamma^4}\frac{v_0^2}{\Delta v_0^2}} \tag{1.37}$$

where $\Delta v_0 = v_0\Delta x_0/D_h\gamma^2$ is the cross over velocity without beta oscillations. From equation (1.37) we find the cross over position to be

$$\Delta x_0^{\beta} = \frac{1}{2}\Delta x_0 + \frac{1}{2}\Delta x_0\sqrt{1 - \frac{2\epsilon_h\beta_h}{\Delta x_0^2}} \tag{1.38}$$

We observe from the calculations that the cross over velocity offset falls with increasing emittance. This means that we can calculate a critical emittance above which the particles will be heated rather than cooled. This emittance is the emittance at which the friction force only has one zero point.

$$\epsilon_h^{crit} = \frac{\Delta x_0^2}{2\beta_h} \tag{1.39}$$

which for the systems shown in Table 1.4 are calculated in Table 1.6.

Machine	I_e	ϵ_h^{crit} [π mm mrad]
LEAR, 96-1, Pb. beam at 4.2 MeV/nucl.	0.3 A	18
LEAR, 96-1, Protons at 310 MeV/c	1.0 A	$2.1 \cdot 10^3$
AD, (Anti)protons at 300 MeV/c	2.5 A	$3.9 \cdot 10^4$
AD, (Anti)protons at 100 MeV/c	0.3 A	$4.9 \cdot 10^3$

Table 1.6: Critical emittances for various machines. Theoretically particles with emittance above the critical are heated, not cooled, for any longitudinal velocity offset.

Earlier we also studied the influence of displacing the electron beam and ion beam with respect to each other; this calculation would also be more accurate if we include the betatron oscillations. The correction to the displacement cut off becomes

$$\Delta x_{cut}^{\beta,e} = \Delta x_{cut}^{e}\left(1 - \frac{2\epsilon_h\beta_h}{\Delta x_0^2}\right) \tag{1.40}$$

which in contrast to Δx_0^{β} is linear in ϵ_h.

By displacing the electron beam in the positive x-direction, larger critical emittances than those given in table 1.6 result.

1.4.2 Vertical Betatron Oscillations

In the vertical dimension we do not have dispersion in the ion beam, but the electron beam velocity profile is as in the horizontal dimension. The longitudinal velocity offset from the electron beam with both vertical and horizontal emittance becomes

$$\Delta v_{\parallel}^{\beta}(\phi) = \Delta v_{\parallel} - v_0 \cdot \frac{\Delta v}{v}\left(\sqrt{\left[D_h\gamma^2\frac{\Delta v_{\parallel}}{v_0} + \sqrt{\epsilon_h\beta_h}\sin\phi\right]^2 + \epsilon_v\beta_v\sin^2\psi}\right) \tag{1.41}$$

where ψ is the phase of the vertical oscillation, assumed uncoupled to the horizontal. This results in the following simple change of equation (1.36)

$$F_{\parallel}^{\beta}(v_{p,\parallel}) = -\frac{4\pi\eta n_e Z^2 r_e^2 m_e c^4 L_C}{v_p^3}\left[v_{p,\parallel} - \frac{I_e v_0}{8\pi\epsilon_0\beta c a^2\Phi_0}\left(D_h^2\gamma^4\frac{v_{p,\parallel}^2}{v_0^2} + \frac{1}{2}\{\epsilon_h\beta_h + \epsilon_v\beta_v\}\right)\right] \tag{1.42}$$

thus the cross over point is changed to

$$\Delta x_0^{\beta_\perp} = \frac{1}{2}\Delta x_0 + \frac{1}{2}\Delta x_0\sqrt{1 - \frac{2(\epsilon_h\beta_h + \epsilon_v\beta_v)}{\Delta x_0^2}} \tag{1.43}$$

and the cut off displacement is

$$\Delta x_{cut}^{\beta_\perp,e} = \Delta x_{cut}^{e}\left(1 - \frac{2(\epsilon_h\beta_h + \epsilon_v\beta_v)}{\Delta x_0^2}\right) \tag{1.44}$$

1.5 Misalignment of the electron beam

In this section we consider the influence of various misalignments between the electron beam and the circulating particles.

1.5.1 Offsets

We have already considered the influence of horizontal offsets, and, related to it, the so-called cutoff position, which is the horizontal offset at which no cooling will occur, because the relationship between the electron and the ion velocities are such that the ions will be accelerated out of the acceptance of the machine due to the lattice dispersion in the electron cooler.

In the case were we have no dispersion for the ion beam in the electron cooler, the situation in the horizontal and the vertical plane is identical. An offset between ions and electrons will result in the probing of a different fraction of the electrons. If the ion beam is much smaller than the electron beam this will only lead to a small change in the cooling time, which is caused by the increased initial velocity difference between the circulating beam and the electron beam. The increased initial velocity difference stems from the changes in the electron velocity across the electron beam. At some point, depending on the relative sizes of the two beams parts of the ion beam will no longer overlap with the electron beam, and the cooling time will increase rapidly hereafter. To have a notion of the magnitudes involved, we have in Table 1.7 calculated the ion beam sizes, and the maximum offset possible with complete overlap with the electron beam.

Machine	ϵ_i^h [mm mrad]	r_i^h [mm]	x_{max} [mm]	ϵ_i^v [mm mrad]	r_i^v [mm]	y_{max} [mm]
LEAR, 96-1, Pb., 4.2 MeV/A	40π	8.7	16.3	10π	8.0	17.0
LEAR, 96-1, p, 310 MeV/c	40π	8.7	16.3	10π	8.0	17.0
AD, $\bar{p}$ at 300 MeV/c	33π	16	9.0	33π	14	11.0
AD, $\bar{p}$ at 100 MeV/c	6π	6.9	18.1	6π	5.9	19.1

Table 1.7: Ion beam emittances, equivalent sizes (2σ) and maximum offset with full overlap with the electron beam for the initial emittance in 4 standard situations for both the horizontal and vertical dimensions. We have assumed an electron beam radius of 25 mm throughout.

Table 1.7 shows that for most of our setups we have reasonable alignment space. However for the setups where we have strong space-charge influence on the electron beam, we will still see deterioration of the cooling even with small offsets. It should also be kept in mind that if *both* dimensions are offset the available space in both dimensions shrink.

1.5.2 Angular misalignment

The dispersive electron and circulating beams also means that with an angular misalignment between the two beams the circulating beam experiences a higher effective electron temperature because part of the longitudinal velocity is now experienced as transverse velocity spread. Another thing is that as in the offset case the physical overlap may be altered, and the cooling time therefore increased. This effect will be further enhanced if there is dispersion in the ion beam, as parts of the electron beam may be offset beyond the cut-off offset. Finally the longitudinal and transverse degrees of freedom of the electron beam are mixed, and as the longitudinal temperature is much smaller than the transverse this may lead to less efficient cooling.

In Table 1.8 we have calculated various numbers, which demonstrate the different effects of angular misalignment. The table shows the maximum angular misalignment, before parts of the ion beam stop being overlapped by electrons and before the offset brings parts of the beam beyond the cut-off displacement. Furthermore it shows a calculation of the angle at which the longitudinal electron temperature is doubled due to mixing with the transverse temperature.

Machine	I_e [A]	$\epsilon_h^{2\sigma}$ [mm mrad]	θ_{max} [mrad]	θ_{cut} [mrad]	θ_{double} [mrad]
LEAR, 96-1, Pb., 4.2 MeV/A	0.3	40π	10.7	-	30
LEAR, 96-1, p, 310 MeV/c	1.1	40π	10.7	7.1	30
AD, $\bar{p}$ at 300 MeV/c	2.5	33π	18.7	125	45
AD, $\bar{p}$ at 100 MeV/c	0.3	6π	7.9	44	45

Table 1.8: Various angles corresponding to either the maximum angle possible with total overlap, angle at which some part of the electron beam is offset with the cut-off offset, and angle at which the effective longitudinal velocity spread is doubled. Note that for the 4.2 MeV/A Lead beam the initial emittance is beyond the critical (see Table 1.6).

From the numbers we may deduce that only for the lead experiments was the angle possibly an important factor, as we are already in a critical situation with the initial emittance. The values are just to give an estimate, naturally a displacement of the beam or increased electron currents will change the picture. We should also keep in mind that in the experiments the control is limited, and therefore we may have both angular and position misalignments, and these effects together may enhance any undesirable effects.

Chapter II

Experiments with cooling

In 1996 and 1997 a series of experiments were carried out at LEAR in order to investigate the electron cooling time under various circumstances [6]. The measurements were carried out with several different magnetic lattices, some having dispersion at the electron cooler and some not. The dependence of the cooling time on the electron current, and the lattices, as well as horizontal offset between the cooling electron beam and the circulating beam was investigated. The experiments were carried out both with protons and Lead ions.

In this chapter we will briefly review a few of the results, as we will use these as reference for cooling simulations using the program BETACOOL [5]. The purpose of this is to establish to which extent the program can be expected to simulate reality.

2.1 Lattice and beam specifications

The different lattices (here called machines) used for the experiments had the characteristics of interest for the simulations (which do not consider the collective effects in the circulating beam, and therefore do not need the full lattice) listed in table 2.1. The characteristics of the proton and lead ion beams as well as the cooler settings are given in Table 2.2.

		Machines used up to 1996 ['Machine #']				Machines used in 1997 ['Machine #']		
		96-1	96-4	96-6	96-7	97-0	97-1	97-2
Twiss parameters at the Cooler	β_h [m]	1.9	9.5	0.65	4.8	5.0	5.0	5.0
	β_v [m]	6.4	10.5	5.5	5.0	5.0	5.0	5.0
	D_h [m]	3.6	0	0	5.0	0.0	-1.0	-2.0
Working point	Q_h	2.31	1.62	2.76	2.55	1.59	1.59	1.59
	Q_v	2.62	2.42	2.72	2.70	2.57	2.57	2.57
Transition	γ_T^2	-39	8.1	8.1	-28	8.1	18	-33

Table 2.1: Lattice functions for the optical settings of LEAR used in the experiments.

	Lead Ions	Protons
Kinetic Energy	4.2 MeV/nucl.	50 MeV
Velocity factor $\beta = v/c$	0.095	0.31
Storage ring circumference	78.54 m	78.54 m
Initial energy spread Δp/p	$1{\cdot}10^{-3}$	$2{\cdot}10^{-3}$
Initial horizontal emittance ϵ_h	40 π mm mrad	40 π mm mrad
Initial vertical emittance ϵ_v	10 π mm mrad	10 π mm mrad
Kinetic Energy of cooling electrons	2.3 keV	27 keV
Longitudinal E-beam Temp.	$1{\cdot}10^{-4}$ eV	$1{\cdot}10^{-4}$ eV
Transverse E-beam Temp.	$\sim$ 0.1 eV	$\sim$ 0.1 eV
Cooling length l_e (< 1997)	1.5 m	1.5 m
Cooling length l_e (= 1997)	3.0 m	3.0 m
Electron beam radius a_e	25 mm	25 mm
Electron currents I_e	0.05 - 0.4 A	1 - 2.2 A
Magnetic field in cooler B	0.06 T	0.06 T

Table 2.2: Main parameters of the beams and the corresponding settings of the electron cooler.

2.2 Measurements

Each measurement was carried out by optimizing both the energy of the electron beam and the relative position as well as angle of the electron beam to the beam to be cooled. The cooling time was measured as the time it took to cool the horizontal emittance from 40π mm mrad to 4 π mm mrad.

It should beforehand be noted that there were no direct means by which to monitor the relative alignment of the electron beam to the circulating ions. But in all measurements care was taken to minimize the cooling time in each measurement series by adjusting the alignment.

2.2.1 Lead ions

Figure 2.1 shows the cooling rates for various lattice settings (machines) as a function of the electron beam current. Each point in the graph is an average over several measurements, and was the optimum cooling rate obtainable at that specific current setting. The cooling was optimized by optimizing the accelerating voltage of the electron beam and by optimizing the electron beam / ion beam overlap.

For lead ions at 4.2 MeV/nucl. the simple approximations in section 1.1 can be used to estimate the cooling time. The results from these equations depend only weakly on the beta functions, and not at all on the dispersion. The cooling down time can be written

$$\tau_\perp = 0.38 \text{ sec} \cdot \frac{0.3A}{I_e} \tag{2.1}$$

where ϵ_h = 40 π mm mrad, ϵ_v = 10 π mm mrad, L_{ecool} = 1.5 m and $T_{e,\perp}$ = 0.11 eV has been

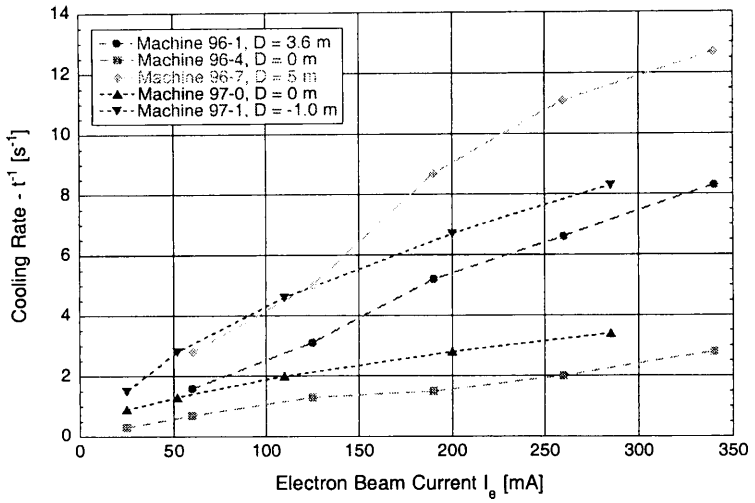

Figure 2.1: Measured cooling rates of Pb ions as a function of electron beam intensity for different lattice parameters at the electron cooling device. The values of the lattice parameters are given in table 2.1. Note that for the 97 machines L_{cool} is twice the value for the 96 machines.

assumed. The variation with emittance is small (about +10% if $\epsilon_h = 4\ \pi$ and $\epsilon_v = 1\ \pi$).

Comparing the simple estimate to the experiments we conclude that the order of magnitude is reasonable, and we observe to a large extend the expected inverse proportionality of the cooling time to the current. However, the variations with dispersion and beta functions are large. More detailed calculations are therefore necessary to make useful predictions.

We can get a first impression of the influence of dispersion by calculating the cross over points between cooling and heating (equation (1.27)), as well as the temperature, equation (1.25), corresponding to the space charge induced velocity spread.

Figure 2.2.a shows the temperature of a dispersive electron beam (equation (1.25)) for an electron beam with a kinetic energy of 2.3 keV (corresponding to a lead kinetic energy of 4.2 MeV/nucl.). As we can see the induced velocity spread is significant compared to the natural longitudinal velocity spread of the electrons. However, influence on the transverse cooling is mainly to be expected when the longitudinal temperature becomes of the same order as the transverse, which happens when the current is between 0.2 and 0.8 Amperes - thus in this regime we would expect to see an increase in the cooling time compared to the scaling given by equation (2.1). If on the other hand we have a magnetized electron beam the determining temperature is the longitudinal electron temperature, and space-charge becomes important for a much larger range of currents.

Using equation (1.27) we can also calculate the cross over point between heating and cooling as a function of current. In this case we would be interested in whether the cross over distance is comparable to the size of the ion beam (initial or final).

Figure 2.2.b shows the cross over point as a function of the electron beam current for two different values of dispersion (corresponding to machine 96-1 and 96-7) . For comparison we can calculate the horizontal beam sizes (2σ) for initial and final emittances (40π and 4π respectively) for the different machines. This is shown in Table 2.3.

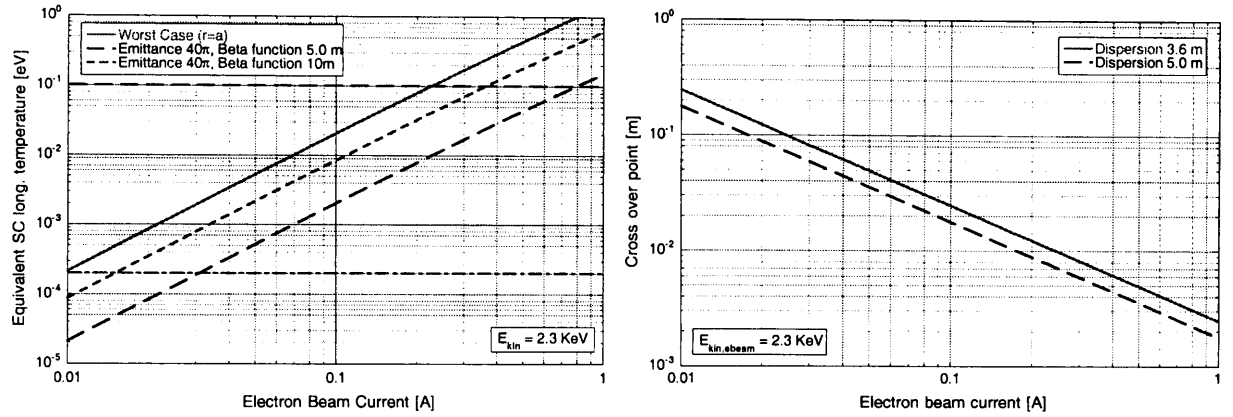

Figure 2.2: LEFT: Equivalent longitudinal temperatures (in meV) of an electron beam with space-charge induced dispersion. The three lines correspond to considering either all of the electron beam (worst case), or only a part of it corresponding to the size of the ion beam (2σ). The horizontal lines give the transverse (dashed) and longitudinal (dot-dashed) temperature of the electron beam. RIGHT : Cross over point as a function of electron beam current for cooling of lead ions.

Beam size in electron cooler				
	Machine Lattice			
Emittance	96-1	96-4	96-6	96-7
Initial (40π)	$8.7{\cdot}10^{-3}$ m	$1.9{\cdot}10^{-2}$ m	$5.1{\cdot}10^{-3}$ m	$1.4{\cdot}10^{-2}$ m
Final (4π)	$2.8{\cdot}10^{-3}$ m	$6.0{\cdot}10^{-3}$ m	$1.6{\cdot}10^{-3}$ m	$4.4{\cdot}10^{-3}$ m

Table 2.3: Initial and final horizontal beam sizes (2σ) for comparison with the cross over points.

Comparing the beam sizes with the cross over points we see that for the machines with dispersion (96-1 and 96-7) the largest beams have $2\sigma \sim 10^{-2}$ m, which is comparable to the cross over point for currents of 0.2A - 0.3A. The maximum current possible in the experiments before cooling failed was about 0.35A, which is in good agreement with these estimates.

2.2.2 Protons

With the proton beam the cooling-down time was measured as a function of the horizontal offset between the electron beam and the proton beam. Figure 2.3 shows the cooling-down time measured for various machines as a function of the horizontal offset.

As before we can estimate the cooling down time using equation (1.6)

$$\tau_{\perp} = 3.2 \text{ sec} \cdot \frac{1.1A}{I_e} \tag{2.2}$$

where ϵ_h = 40 π mm mrad, ϵ_v = 10 π mm mrad and L_{ecool} = 3.0 m has been assumed.

This estimate does as before not include dispersion, which as we can see in Figure 2.3 is important. As before the order of magnitude is right (for zero displacement), but there are again large variations as a function of dispersion which are not accounted for by the simple calculation.

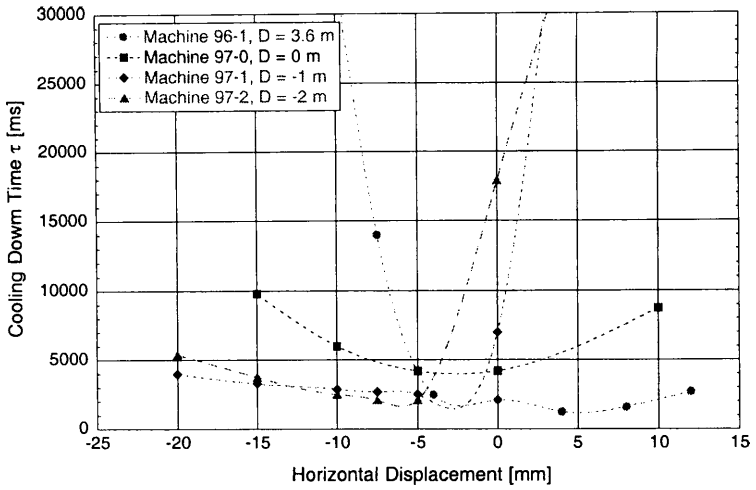

Figure 2.3: Cooling down times (ϵ_h : 40 π $\rightarrow$ 4 π) for protons at 50 MeV (initial $\Delta p/p = 2{\cdot}10^{-3}$) as a function of the horizontal offset between the electron and proton beams. The electron beam current was 1.1 A.

The dispersion dependence observed in Figure 2.3 confirms the expected behavior as we approach the cross over point between heating and cooling. We observe that the sign of the position offset where the sudden sharp increase in cooling time appears depends on the sign of the dispersion. The scaling of the absolute magnitude of the offset with dispersion is harder to extract as we have very few points, and because the zero relative displacement of electron beam relative to proton beam is not determined very precisely, a fact which may also account for the slight asymmetry in the plot.

For comparison we have calculated the cross over point as a function of dispersion for a 50 MeV proton beam in LEAR with an electron beam current of 1.0 A. The result is shown in Figure 2.4.

Figure 2.4 indicates that for machine 96-1 with a dispersion of 3.6 m longitudinal cooling will cease with a displacement of $\sim$ 2 cm. In the experiments (figure 2.3) we observed this effect at about 0.5-1.0 cm, and thus smaller. Including transverse betatron motion (equation (1.44)) gives, with emittances of ϵ_h = 40 π mm mrad and ϵ_v = 10 π mm mrad, a correction of -4% to the cut off position. This correction is not large enough to comply with the observations. Furthermore we observe from the calculation of the cross over point that we do not expect pronounced effects of small displacement with dispersions of 1 and 2 meters, contrary to what can be seen in Figure 2.3. In Ref. [6] a measurement of the electrical potential across the electron beam for a 27 keV electron beam is shown. The dispersion in the electron beam extracted from this measurement corresponds perfectly to what we would expect, thus we have no simple explanation for the large position dependence observed in Figure 2.3. However, there is a mechanism which may enhance the effect. As we can see from Figure 2.3 the dependence of the cooling time on position offset for zero dispersion is very weak - this means that we could have a comparatively large offset in the vertical dimension. This would not be easily detectable from the cooling time for zero horizontal offset, but would cause the relative overlap of the electron and proton beam to change

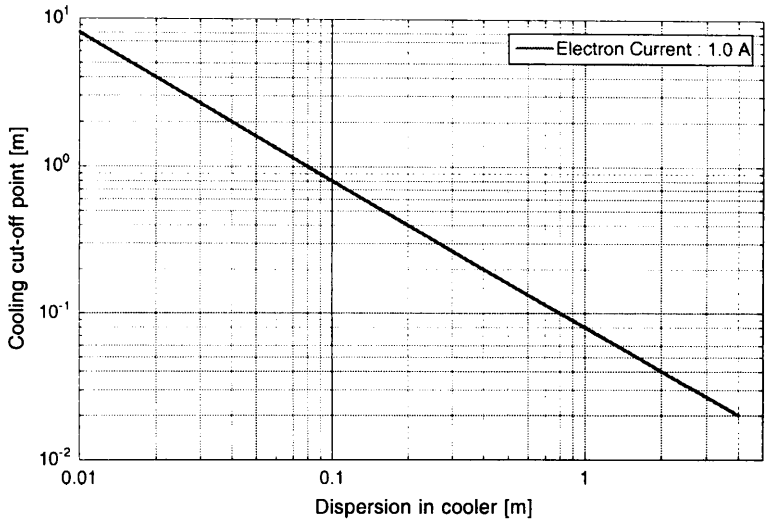

Figure 2.4: Cooling cut-off point (absolute value, equation (1.28)) for a 50 MeV proton beam in LEAR as a function of dispersion in the electron cooler.

faster than if the vertical overlap had been good, and the edge effects would be more pronounced. Unfortunately this could not be investigated in these measurements, but it is a plausible reason for the apparent reduction of the horizontal electron beam size, and we will return to it in the simulations to investigate the possible magnitude of this effect.

Chapter III

Simulations of cooling

In this chapter we analyze the outcome of electron-cooling simulations. First we discuss how to run and interpret the results of the used simulation program, and secondly we use the program to simulate the experimental data discussed in the previous chapter, in order to establish how well the simulations can reproduce experimental data, and thus to what extent we can use it to predict future cooling results.

3.1 The simulation software

For the simulations we have used the program BETACOOL [5] which simulates cooling of a circulating particle, with specific initial conditions. The cooling force from the electron beam is calculated using an extended version of equation (1.1), which is given as equation (1.36) in reference [7] (including both the expression for longitudinal and transverse friction). This friction includes the effect of magnetization of the electron beam. Therefore the program includes an option for invoking the influence on the ion motion of a longitudinal magnetic field in the cooling section and furthermore one can activate compensation solenoids to cancel the mixing of the transverse motion of the ions. The dispersion in the electron beam due to space-charge as well as the induced $E \times B$ drift is also included, the latter as an increase of the transverse thermal velocity of the electrons.

The program does not include intra-beam scattering in the electron beam or the ion beam. Furthermore it does not include the heating of the electrons by the ion beam. Of these effects only IBS in the circulating beam is expected to be significant, as the other effects were found to be weak in chapter 1, and this can be calculated using a program called INTRABTC [10].

The input parameters required are listed in Table 3.1

In the program the initial position of the particle in transverse phase space cannot be input. Rather the program starts the particle by assuming that it has zero position error and maximum divergence error. Thus the initial conditions for a particle are for the horizontal phase space (0, $\sqrt{\epsilon_h \gamma_h}$) and for vertical (0, $\sqrt{\epsilon_v \gamma_v}$). As the measurements are all for coasting beams we ignore longitudinal bunching and do the calculation for a given initial $\delta p/p$, but note that the cooling may depend on the sign of the velocity offset of the particle from the electron beam velocity (if

Ion Beam Parameters	Ring Parameters	Cooler
Energy pr. nucleon	Ring Circumference	E-Beam current
Atomic Number	β_h at cooler	E-Beam radius
Charge	β_v at cooler	Longitudinal B-field
Initial "H-Emittance"	$d\beta_h/ds$ at cooler	$T_\perp$ in meV
Initial "V-Emittance"	$d\beta_v/ds$ at cooler	$T_\parallel$ in meV
Initial momentum deviation	Dispersion at cooler	Cooler Length
	Horizontal Tune	H/V position offset of beam
	Vertical Tune	H/V angle offset of beam
		Compensation solenoids

Table 3.1: Main input parameters for the program BETACOOL. It is also possible to specify a neutralization of the e-beam. As this feature is not used here it has not been listed.

there is dispersion).

In an older version of the program it was possible to input the detailed initial conditions, and a simple investigation varying the initial conditions in accordance with the specified "emittance" reveals that the cooling time can differ up to typically no more than $\pm$ 10% with varying initial phase space positions (in only pathological cases where the electron current is high and the ion beam size and dispersion are such that one can start close to the cross over point, equation (1.27), there may actually be initial conditions where the particle is not cooled at all).

3.2 Interpretation of simulation results

As the program deals with single particles we need to consider how to interpret the results in order to obtain estimates for the cooling time of a *beam* of particles. We are interested in the cooling down time of a beam of $\epsilon_h = 40\ \pi$ mm mrad and $\epsilon_v = 10\ \pi$ mm mrad to $\epsilon_h = 4\ \pi$ mm mrad. We consider the time it takes to cool down particles with a horizontal "single particle emittance" 40 π mm mrad, which thus gives the time it takes to cool down 95% of a beam of 2σ emittance 40 π mm mrad. However, we need to take the longitudinal momentum spread as well as the vertical emittance into account. This can be done by a weighted average over the cooling down times of $\epsilon_h = 40\ \pi$ mm mrad particles over the possible initial vertical single particle emittances and longitudinal momentum offsets. Thus a realistic estimate for the cooling down time for a Gaussian beam with vertical emittance 10π should be given by

$$t_{cooltime} = \frac{2}{2\pi\sigma_v^{10\pi}(\Delta p_0)} \cdot \int_{-\infty}^{\infty}\int_{0}^{\infty} t_{prg}(y,\Delta p)\exp\left(-\frac{y^2}{2(\sigma_v^{10\pi})^2}\right)\exp\left(-\frac{(\Delta p)^2}{2(\Delta p_0)^2}\right) dy\, d(\Delta p) \quad (3.1)$$

where $\sigma_v^{10\pi}$ is the RMS beam size of a beam with a 2σ vertical emittance of 10π, and where the vertical amplitude y of a particle is given in terms of the single particle emittance ϵ_v as

$$y = \sqrt{\beta_y \cdot \epsilon_v} \quad (3.2)$$

Invoking this integral for each is however very time consuming, and with the expected accuracy most likely not worth it. However, we will for some cases investigate the changes with initial vertical single particle emittance and initial longitudinal momentum offset.

In order to avoid confusion in the following it should be noted that from now on emittance when related to the program means "single particle emittance", and thus gives the amplitude of the particle directly (eqn. (3.2)), rather than the RMS position which is a factor $1/\sqrt{2}$ times the amplitude.

3.2.1 Vertical Emittance

First we have investigated how the cooling down time depends on the vertical emittance under various conditions, and machines. Figure 3.1 shows the dependence of the cooling down time on the initial vertical emittance for two different initial momentum offsets, in order to be sure that the momentum offsets (which we will investigate shortly) do not influence the conclusions. The figure shows the results for two different beam currents and for two different machines which have vertical beta functions of 5-6 m at the cooler.

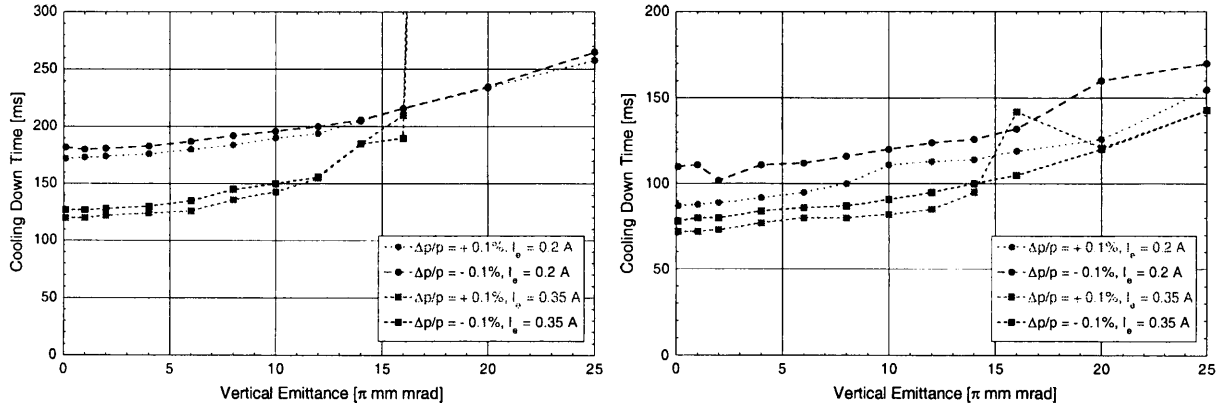

Figure 3.1: Cooling down times from simulations for Pb^{54+} ions at 4.2 MeV/u. Left: Machine 96-1 used with $T_{\perp}^{ebeam}$ = 140 meV. Right: Machine 96-7 with $T_{\perp}^{ebeam}$ = 100 meV. The small difference in transverse temperature is in order ot match the measured data better as discussed later in the text.

Figure 3.1 shows that the cooling down time of the horizontal emittance only depends relatively weakly on the vertical emittance for the two different machines tested here. This indicates that extracting a cooling down time for a beam from the single particle simulations can be done with good precision without simulating for a range of different initial vertical emittances. However, as we will see in Figure 3.2.a, we observe large variations in the cooling down times for machine 96-4, and also large difference between positive and negative initial momentum offset. But before going into details on this behavior we should comment on the sudden increase in cooling time in Figure 3.1.a for I_e = 0.35 A at an emittance of 17 π mm mrad. What is in fact observed is that above about 13 π mm mrad the emittances and momentum offset no longer converges to zero, but rather to some finite value. At about 16π, this finite emittance is larger than 4π mm mrad and we therefore have and 'infinite' cooling down time.

To understand this we observe that for the given settings the theoretical cross over point is Δx_0 = 7.0 mm. A vertical emittance of 13π mm mrad corresponds to an amplitude of 9 mm, which corresponds to a velocity offset in the electron beam of 0.3%. The amplitude (of the *one* simulated particle) corresponding to the horizontal emittance of 40 π mm mrad is 8.8 mm in the cooler. The vertical amplitude at 16 π mm mrad is 10 mm. From these conditions we observe that we are beyond the 'bare' cross over point initially, i.e. the cross over point with zero transverse emittance. Thus the averaging between cooling and heating caused by the betatron motion results in an increased value for the cross over point. This indicates that the friction force is in a regime where it is inversely proportional to the velocity, as linear friction caused decreased value for the cross over point (see section 1.4). We will return to this later in this chapter.

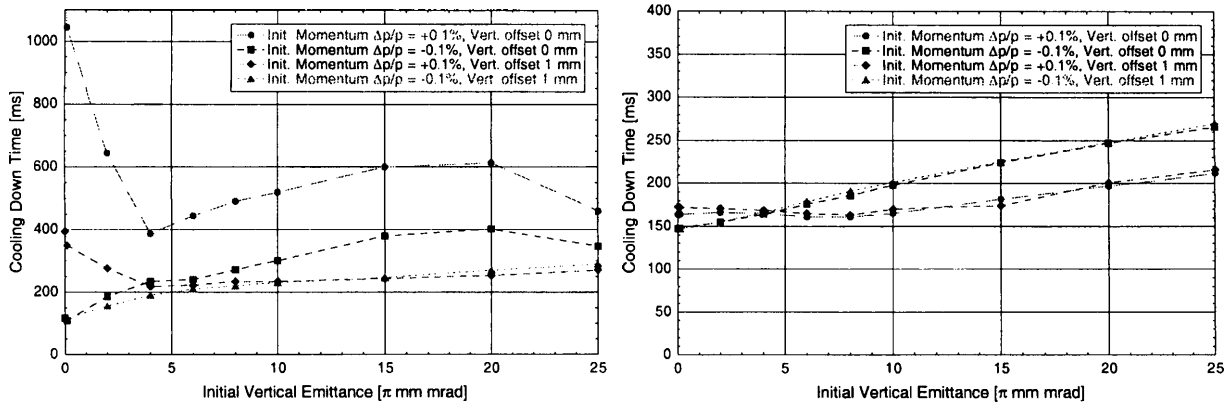

Figure 3.2: Cooling down times from simulations for Pb^{54+} ions at 4.2 MeV/u. Machine 96-4 used with $T_{\perp}^{ebeam}$ = 140 meV and 0.2 A (left) and 0.1 A (right) electron beam current. The simulation was done with two different vertical beam-beam offsets.

Returning to the issue of the generally weak dependence of the cooling down time on the vertical emittance, we investigated the behaviour of Machine 96-4 under various circumstances as shown in Figure 3.2. We observe that for a current of 0.2A, with perfect alignment of the electron and ion beam the difference between positive and negative initial momentum offset is large, and the variation in the cooling down time is large as a function of the vertical emittance. This is disturbing for the previous conclusions, but a small misalignment in the horizontal dimension (1mm, compared to a e-beam diameter of 50mm) changes the behaviour drastically, and we observe that for lower currents (Figure 3.2.b) the variation in the cooling down time both with and without offset is much less. This behaviour does not invalidate the previous conclusions that we can use only one point in the emittance, but it means that before drawing conclusions on a simulation we need to investigate all possible parameters in order to be sure that the simulation results are 'stable'.

The reason for the stange behaviour of machine 96-4 is not clarified in this discussion, but Machine 96-4 is very different from the other two in that the beta functions at the cooler are large, thus the cooling will be more sensible to the electron velocity distribution across the electron beam. Furthermore the lattice dispersion in the electron cooler is zero. We investigate different aspects of this behaviour further in the coming sections.

To summarize the results of this section: we observe a weak dependence of the cooling down time on the initial vertical emittance, which means that we will not bother to make averages of various vertical emittances from now on. However, we have also observed that we should be careful before drawing conclusions as some configurations may be very sensitive to initial conditions.

3.2.2 Longitudinal Momentum Spread

In the next series of simulations the initial longitudinal momentum deviation of the simulated particle was varied in a range relevant to the experiments (which supposedly had initial longitudinal momentum spreads of $\sim 0.1\%$). At the same time all other parameters were kept constant with values in reasonable agreement with the experimental data (i.e. the transverse electron temperature was varied in order to fit the cooling time observed in the experiments).

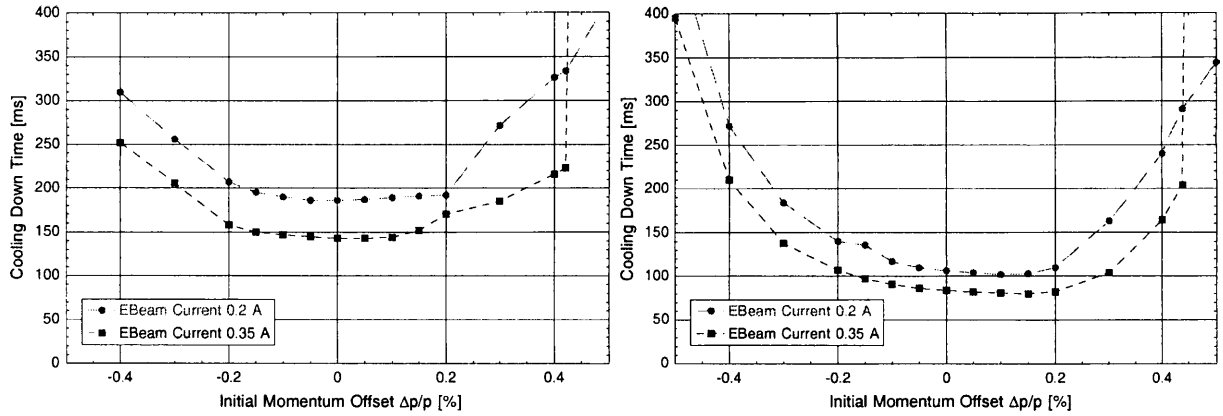

Figure 3.3: Cooling down times from simulations for Pb^{54+} ions at 4.2 MeV/u. Left: Machine 96-1 has been used with a transverse electron beam temperature of 140 meV. Right: Machine 96-7 has been used with a transverse electron beam temperature of 100 meV. The simulated cross over point is $\Delta p = 0.421$ and $\Delta p = 0.438$ respectively. Initial vertical emittance is 10 π mm mrad.

As before we first look at machines 96-1 and 96-7. Figure 3.3 shows the horizontal cooling down time as a function of the initial momentum offset for two different electron beam currents for machines 96-1 (Fig. 3.3.a) and 96-7 (Fig. 3.3.b). We observe that the larger the initial momentum the longer the cooling down time. This is to be expected, as the cooling time depends on the total velocity difference between the electrons and the ions, and larger initial momentum spread means larger relative velocity. Due to the dispersion in the electron beam and in the ion beam there is an asymmetry around zero momentum offset, in agreement with the discussion in section 1.2.

At a certain initial momentum offset there will no longer be cooling in the longitudinal dimension, but rather heating, as we discussed in section 1.2. This of course means that the transverse dimensions will not be cooled either. In the simulations (Figure 3.3) we observe this effect as the beam never reaching the horizontal emittance of 4 π mm mrad, which we have indicated as infinite cooling time in the plots. According to equation (1.27) the cross over momentum offset

for machine 96-1 and 96-7 with Pb should be 0.2%, and 0.15% respectively. In the simulations we observe 0.421% and 0.438% for machine 96-1 and 96-7 respectively. The simple calculation is thus about a factor of 2 to 3 wrong compared to the simulation. However the simple calculation has neither included betatron oscillations as discussed in section 1.4 nor magnetic effects. We observed in chapter 1 that magnetic effects in the 96 Pb machine may be important, and when they are, the betatron oscillation influence changes sign (in section 1.4 we assumed linear friction), and we obtain larger cross over momentum offsets as observed. Thus there seems to be reasonable agreement between the simulations and our theoretical expectations.

Finally we observe that the variation in cooling time with momentum is very weak in the range ± 0.1%, which means that we can use simulations with only one initial setting for predictions. However, in order to compensate for the asymmetry, which is more pronounced when the electron current is high, we choose to use cooling times which are the average value of the simulated cooling down time with initial momentum +0.1% and -0.1%.

In the previous section we observed that machine 96-4 behaved differently from the other two 96 machines. Therefore we again take a look at this machine. Figure 3.4 shows the variation in cooling time for machine 96-4 as a function of the initial momentum offset of the particle.

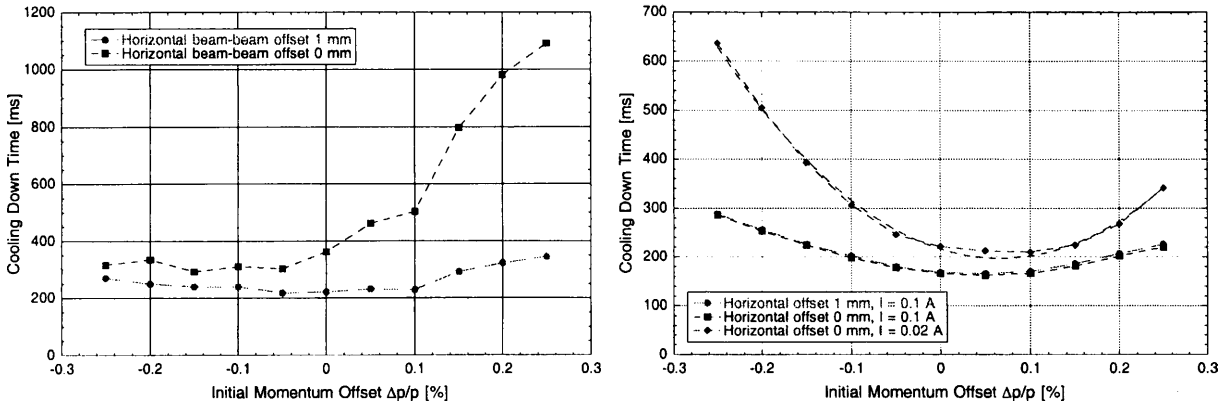

Figure 3.4: Cooling down times from simulations for Pb^{54+} ions at 4.2 MeV/u. Machine 96-4 used with $T_{\perp}^{ebeam}$ = 140 meV. In the left plot the electron current was 0.2 A. The initial vertical emittance was 10π mm mrad.

In Figure 3.4.a we observe that with an electron current of 0.2 A the dependence of the cooling down time on the initial momentum offset is strong and asymmetric. However, as we observed previously at small horizontal displacement, which at lower currents (Figure 3.4.b) is not significant, changes the dependence dramatically. Thus the simulations show again a high sensitivity to the initial conditions, but apart from that, when we do simulations under less sensitive conditions we observe the same behaviour as for the other 96 machines, that is that the variation within an initial momentum offset range of ± 0.1% is small, and can be taken into account by an average between the cooling down time for the two extremes.

Generally we thus observe reasonable agreement with expectations from the analytical estimates, and weak dependence on the initial momentum spread in the ranges where we are far from the cross over point between cooling and heating (non-zero dispersion in the ion beam).

We observe again that care should be taken that we are not in a situation with high sensitivity on the initial conditions.

3.2.3 Lattice parameters

For machines 96-1 and 96-7 the cooling down times varied little, with initial conditions of the particle, whereas machine 96-4 is very sensitive to them. The main difference between these two sets of machines is the lattice function at the cooler. In the 96-4 machine we have large beta functions and zero dispersion, whereas in the other two the beta functions are comparatively small and the dispersion is non-zero.

Figure 3.5 shows the change in the cooling down time as a function of the dispersion at the cooler for all other parameters constant. Two situations have been tested numerically, both the standard machine 96-4 and a modified machine, where the modification consists of a change in the beta function values at the cooler.

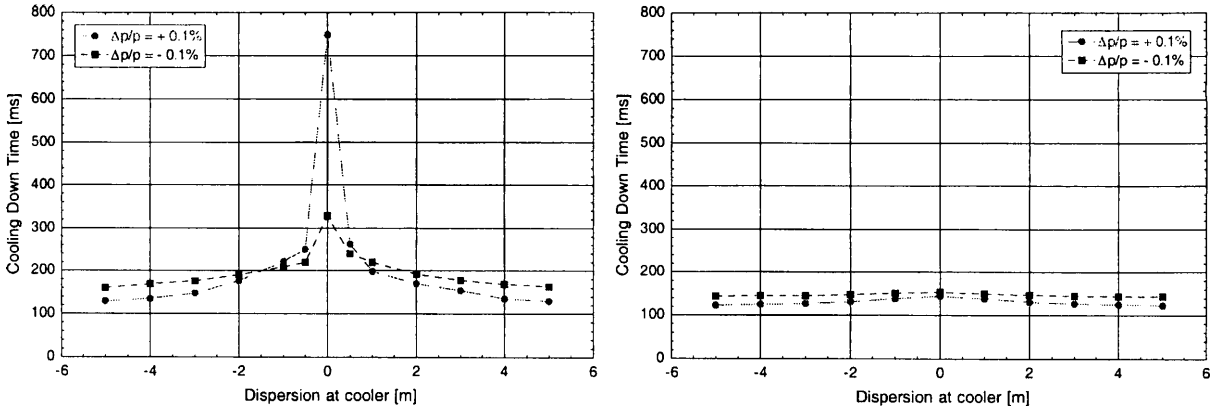

Figure 3.5: Cooling down times from simulations as a function of dispersion for Pb^{54+} ions at 4.2 MeV/u. Left: "Machine 96-4" with β_h = 9.5 m, β_v = 10.5 m and variable D used with a transverse electron beam temperature of 140 meV. Right: A modified machine 96-4 with $\beta_h = \beta_v$ = 5.0 m, otherwise no differences from the simulation displayed in the left plot. The electron current is 0.2 A.

From the figures we learn two things. In the left figure we see that the large discrepancy between the results for opposite momentum offsets disappears when the dispersion is changed away from zero. This indicates that zero dispersion might be a problem. The right figure shows that with smaller beta functions the discrepancy disappears also for zero dispersion, and actually the cooling is in general slightly improved compared to the case with the large beta functions. We therefore conclude that the 'unpredictability' of machine 96-4 is a cumulative effect of zero dispersion and large beta functions.

3.2.4 Summary of the "sensitivity" considerations.

We have from the above investigations learned that we can use the single particle cooling time as a rough estimate for the cooling time. We found small differences in the results as a function

of the initial momentum offset, but as long as the electron beam dispersion and the momentum spread of the beam are not too large it seems adequate to incorporate these differences by just averaging between to offsets of opposite sign. These observations were true for machines with small beta functions at the electron cooler or non-zero dispersion. A machine with zero dispersion and large beta function values showed larger sensitivity to the exact initial conditions, and the cooling time in such a machine might therefore be difficult to estimate. In any case it is recommendable to test the sensitivity to the initial conditions of any machine which one wishes to simulate.

3.3 Comparison with the experiments

In order to make satisfactory simulations it is necessary to find a way to reproduce the measurements without fitting too many parameters. The initial vertical emittance as well as momentum offset and dispersion are parameters that ought to be well know in the experiments. However, the electron temperature is not very well known and may be used as a fitting parameter. The longitudinal electron temperature is very low, and does not alter the results significantly even when changed an order of magnitude, the transverse temperature on the other hand may have a large influence. We expect the transverse temperature to be in the range of 100 - 300 meV.

3.3.1 Electron temperature

In order to quantify this a little we have first looked at how the cooling time depends on the electron beam temperature. Figure 3.6 shows how the average cooling down time of Pb ions at 4.2 MeV/A varies with temperature for simulations with initial momentum offset +0.1% and -0.1%, vertical emittance 10 π mm mrad, and various electron currents.

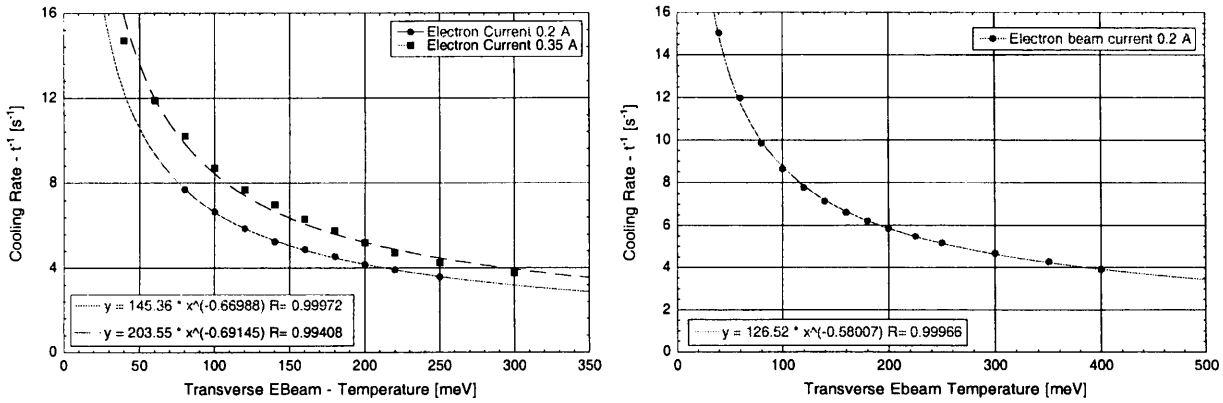

Figure 3.6: Cooling down times for Pb^{54+} ions at 4.2 MeV/u from simulations as a function of ebeam temperature. Left: Machine 96-1. Right: Machine 96-7. Times are averages between times for +0.1% and -0.1%. The lines are power fits to the simulated data.

If we compare the results from the left plot in figure 3.6 to the experiments shown in figure 2.1 we observe that for an electron beam current of 0.2A a temperature of $T_\perp$ = 130 meV gives the

same cooling time in the simulation as in the experiment. At 0.3A the correspondence is better at a temperature of $T_\perp$ = 110 meV. Thus it seems that the electron temperature may change with current. This is perhaps not unreasonable as the ion beam was realigned for each current, and the ion-electron residual misalignment adds to the effective temperature. Thus a detailed investigation has been made in which the temperature was varied at each electron beam current in order to match the experimental data of figure 2.1.

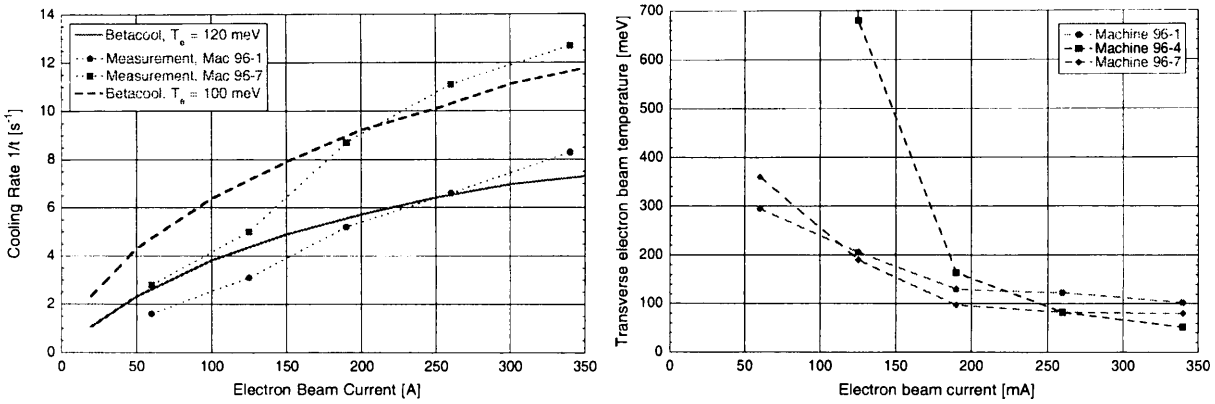

Figure 3.7: Left: Comparisons between simulated cooling times and measured cooling times for the two 'well-behaved' machines. Right: Transverse electron beam temperatures for various currents and machines. The temperature is the value at which the cooling time in the simulation matches the cooling time in the measurement (PB cooling, Figure 2.1).

Figure 3.7.a first shows two examples with the well-behaved machines 96-1 and 96-7 where the electron current has been varied in the simulations and all other parameters kept constant. The cooling down rates are plotted together with the actual measurements and we observe a reasonable agreement, which however suggests that one more parameter may have varied, as discussed above. Figure 3.7.b therefore shows the necessary transverse temperature for matching the simulated cooling rates to the measured for three different machines as a function of electron current. The simulated cooling times were calculated as an average between a simulation with $\Delta p/p$ = +0.1% and one with $\Delta p/p$ = -0.1%.

We observe that for high electron currents the effective transverse temperatures are all of the order of magnitude of 100 meV. At low currents machine 96-4 deviates from the other two. We earlier saw that machine 96-4 was rather sensitive to the initial conditions thus this is perhaps not surprising. However all machines show a tendency for the temperature to rise for lower currents. This is surprising as one might expect that higher currents which generally lead to stronger interaction with the surroundings should cause increased temperature.

In another perspective we could consider what this means if we assume that the temperature was constant in the experiments, or increasing with current. The simulations would then indicate that either the cooling at high currents in the experiments is much better than the simulations indicate or the cooling in the experiments is worse than expected at low electron beam currents. One feature which the program ignores is intra-beam scattering in the ion beam. The intra-beam scattering growth rates calculated using INTRABTC are shown in Figure 3.8.

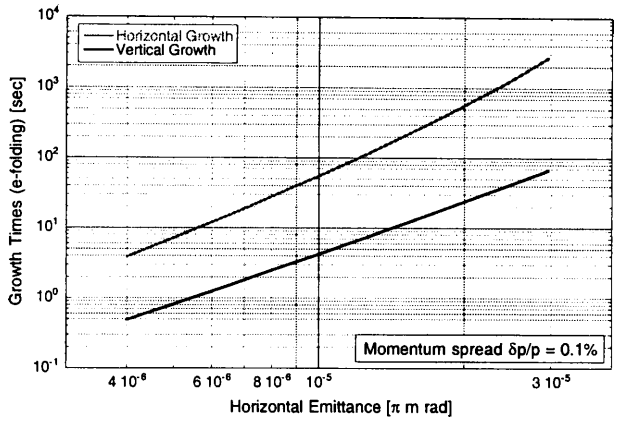

Figure 3.8: Intra-beam scattering calculation for LEAR with a beam of 10^7 Pb ions at 4.2 MeV/nucl. kinetic energy. The vertical emittance (2σ) is 25% of the horizontal during the calculation.

When the electron beam intensity is decreased space charge effects in the electron beam are diminished, but at the same time the friction force of the electron beam is also diminished. When cooling only one particle, as the simulations do, the decrease of the space charge effect will be more important than the diminished cooling power (as there is no IBS-heating), and thus the cooling efficiency will increase with decreased current, exactly as we observe above. In a real beam heating from intra-beam scattering will counteract the cooling and thus lead to longer cooling down times which are obtained in the simulation by higher electron temperatures. As we can see in figure 3.8 the growth times due to intra-beam scattering are on the order of seconds for the final emittances at an intensity of 10^7 Pb ions, and the discussion above may therefore be an explanation for the observed behavior.

3.3.2 Beam-beam overlap

When the measurements were done a lot of effort was spent on optimizing parameters of the system to get the best cooling time. This included the overlap of the electron and ion beam. Before we can be sure of how to model these measurements with the program we need some information as to how sensitive the cooling down time is to the (horizontal) overlap. Figure 3.9 shows two series of simulations for two different machines.

In Figure 3.9 we again see how critical the settings for machine 96-4 are, and therefore how difficult it is to make predictions with this machine. For machine 96-1 the variation as a function of horizontal offset is relatively small, except when the particle is offset enough to be lost due to the dispersion of the electron beam.

As discussed earlier the apparent sudden increase in the cooling time is an illusion and in fact just means that a final emittance of 4π mm mrad can no longer be reached, as the heating of the particle when it is beyond the cut-off is limiting the minimum transverse emittance. For completeness we have also simulated the cooling process as a function of the horizontal angle between the electron and ion beam as well as a function of the vertical displacement. Figure 3.10 shows the cooling down times from simulations as a function of these parameters.

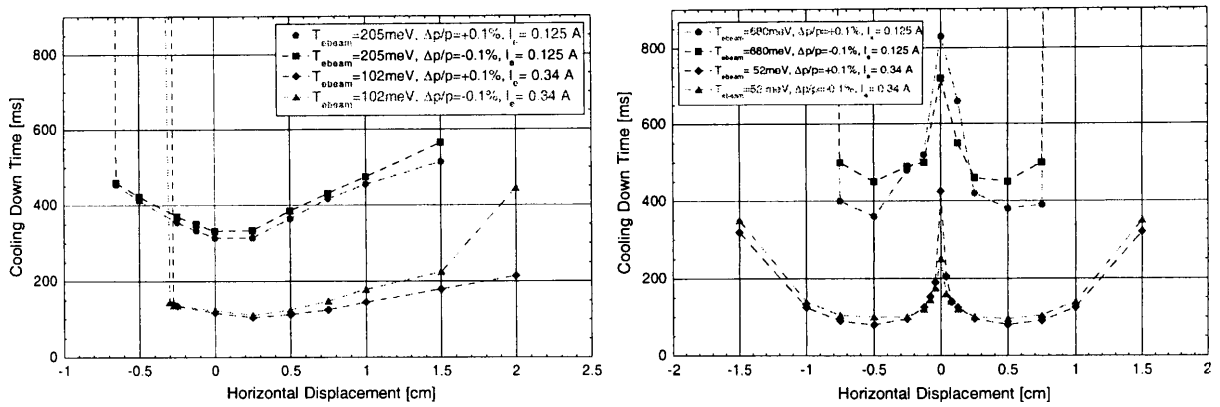

Figure 3.9: Cooling down times from simulations as a function of horizontal offset between electron beam and ion beam. Left: Machine 96-1. Right: Machine 96-4.

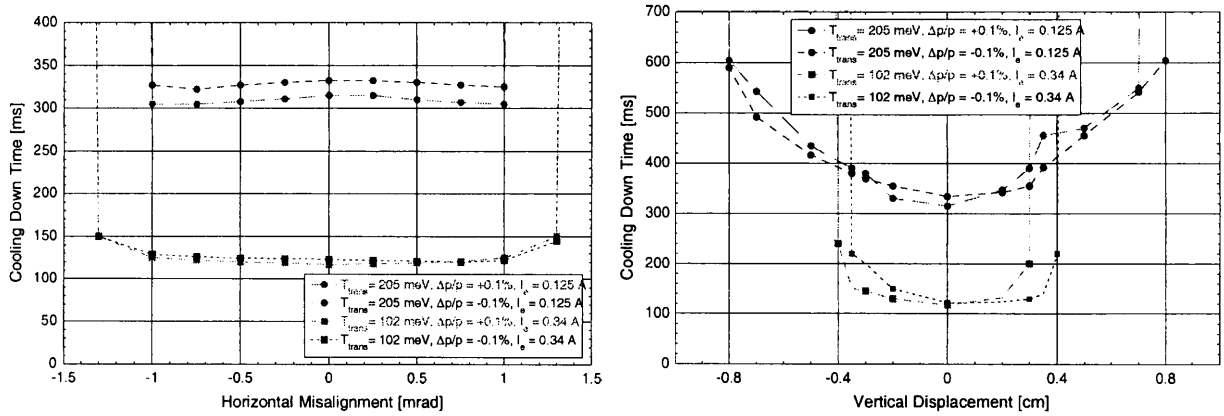

Figure 3.10: Cooling down times from simulations as a function of horizontal angle and vertical displacement between electron beam and lead ion beam in machine 96-1

We observe in Figure 3.10 that the behavior of the cooling as a function of vertical displacement is symmetric around zero displacement, this is because we do not have vertical dispersion in the ion beam. We observe almost zero angle dependence until the point where we can no longer cool down to 4π mm mrad horizontal emittance. We observe that the cooling becomes extremely inefficient at 1.3 mrad (0.34A) and 1.0 mrad (0.125) respectively. The length of the cooling section is 1.5m, thus these angles correspond to a horizontal position change along the beam of approximately 2.0 mm and 1.5 mm respectively. These offsets are of the same order of magnitude as the horizontal offsets where the cooling would be cut off, however they are somewhat smaller, a fact possibly caused by the averaging due to the betatron oscillations.

We have seen that if we wish further insight into the mechanisms causing reduced cooling due to dispersion we need to consider the influence of the betatron oscillations. Figure 3.11 shows the initial momentum offset at which the longitudinal velocity blows up for various transverse emittances. The cutoff-momentum offset has been found using BETACOOL.

Figure 3.11 shows a large influence of the magnetic field on the evolution. The program

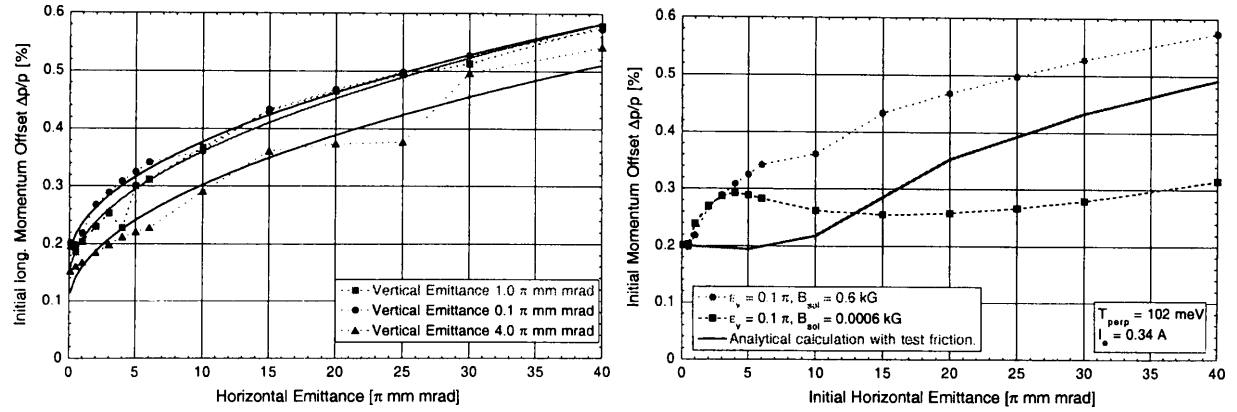

Figure 3.11: Cut-off initial momentum spread as a function of the initial horizontal emittance simulated for a few initial vertical emittances (machine 96-1). The solid lines are squareroot fits to the data. The right plot shows the difference between no magnetic field and 0.6 kG.

BETACOOL has a bug which means that if zero magnetic field is entered the program does not behave right. The cut-off value with almost zero emittance is in agreement with the estimate we have from using equation (1.27), which gives $\Delta p/p = 0.20$ %. However, the dependence on emittance is not what we expect with linear friction (equation (1.37)). We should be in the linear friction regime, as $v_p = \sqrt{v_{p,\|}^2 + v_{p,\perp}^2} = 8.8{\cdot}10^4$ m/s for $\epsilon_h = 40$ π mm mrad and $\delta p/p = 0.2\%$ which is less that $\Delta_\perp = 1.9{\cdot}10^5$ m/s with $T_\perp = 102$ meV, and $\Delta_\| = 4.2{\cdot}10^3$ m/s with $T_\| = 0.5$ meV. However, other calculations in chapter 1 indicated that the magnetic field is important in the 96 machines with Lead, and in that case the linear friction is when the relative velocity is below the longitudinal electron velocity, which we can see from the above estimates that we are not. Thus this indicates the we have an, at least partially, magnetized electron beam. Indications of this were also observed in section 3.2.2.

This assumption can be confirmed by a simple numerical calculation of equation 1.34 with a simple test friction force. The result of calculating the cross over momentum between cooling and heating with horizontal betatron motion with the following friction force,

$$F_\|(v) = -v \frac{1}{1 + \left(\frac{v^2 + v_{p,\perp}^2}{\Delta_\|^2}\right)^{3/2}} \tag{3.3}$$

is shown as a solid line in Figure 3.11.b. The agreement is quite good and we therefore conclude that for machine 96 with lead ions the electron beam and therefore the cooling was strongly influenced by the magnetic field.

3.3.3 Proton Measurements

We have so far mainly discussed the results from lead ion cooling. However in order to establish whether we will be able to make predictions with the simulations concerning the choice of dispersion in the cooling section it is worthwhile with a glance at the proton cooling measurements of the dependence of the cooling on the horizontal displacement as shown in Figure 2.3.

We discussed earlier that it appears that the influence on the cooling down time of horizontal displacement is larger than expected. Using the same procedure at for Figure 3.11 we find that the cross over momentum offset in the simulations at zero emittance corresponds to the momentum at which the lattice dispersion brings the particle outside the electron beam, thus the cross over point is at a larger displacement than the electron beam, as also found in the calculations in Table 1.4. Thus the simulations are in agreement with the simple calculations, but the measurements demonstrated much stronger effects.

These estimates are confirmed by more detailed simulations which cannot reproduce the strong position dependence seen in Figure 2.3. In Figure 3.12 we have shown a series of simulations both with machine 96-1 and the 97 machines, with 50 MeV protons. The figure shows the cooling down times as they were defined in the measurements in figure 2.3. All points are an average between a simulation with an initial momentum offset of +0.2% and -0.2%.

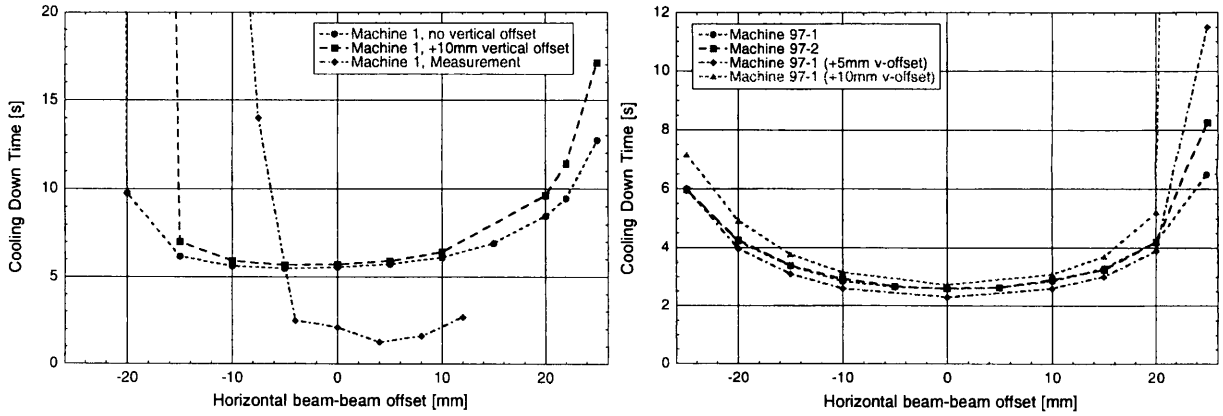

Figure 3.12: Left: Machine 96-1, cooling down time dependence on horizontal and vertical offset between cooling and proton beam (simulations and measurement). Right: 97 Machines. Beam current 1.1 A, Transverse e-beam temperature 140 meV.

Figure 3.12 does not reproduce the measurements very well. The order of magnitude of the cooling in the regions where the cooling seem unaffected by the displacement seems however reasonable (factor of 2 wrong). However, the increase in cooling time as a function of displacement is not large enough for the simulations with zero vertical displacement. We see however that, as discussed in section 2.2.2, a vertical displacement enhances the effect of horizontal displacement. As we at the same time see that for small displacements (below 10 mm) the change as a function of vertical displacement (up to 10 mm) is rather small, it seems plausible that optimizing the displacement via the cooling time is so unprecise that it is possible that the vertical alignment has been rather bad. If we combine these conclusions with the with the previously observed change as a function of angle we may actually have a rather bad alignment in the experiments which only shows up as a strong dependency on the horizontal displacement.

It was proposed by Chanel [11] to do the simulations with twice the emittances assumed in the experiment, in order to see whether this might explain the discrepancy. A simple simulation was carried out to test this hypothesis, and it turned out that the changes as a function of offset were very similar to the changes shown in figure 3.12, and furthermore the cooling times about

doubled. Thus there is no reason to believe that this should be the reason for the discrepancy.

It should finally be mentioned that it is intriguing that the simulations which comply relatively well with the lead measurements are unable to reproduce the proton measurements. There are two possible reasons for this. In the proton measurements the friction forces are much weaker than in the Lead ion case, and this may mean the some of the approximations in the program are too rough, however as the space-charge distribution in the electron beam has been confirmed to match what is expected and the simple estimates of the cross over points are not assuming anything about the friction this seems as the less likely option. The other possibility is that there is something bizarre with the cooler-setup. It is interesting to note that even machine 96-1 with protons does not reproduce in the simulations, whereas it matched quite well with Lead ions. However, one big difference is that all measurements described with protons were carried out with a newly installed cooler, where the solenoid length was twice the old length, thus even though the machine settings were the same the cooler was not. It is surprising that this should lead to cooling times which are consistently better than the simulations suggest at zero offset, but which quickly grows worse with displacement. This indicates that there may have been some kind of unknown new parameter in the new cooler which is not simulated. The strong dependence on offset suggests that this has something to do with the homogeneity of the new setup of its alignment.

3.4 Conclusions

We have looked at how well the simulations reproduce the experimental results, and generally found a reasonable agreement. At the same time we have found that the alignment can be extremely critical, and therefore a source of large possible deviations between simulation and experiment, as it is rather impossible to explore all the available misalignments, which in the experiments may even have changed between single measurements. With this in mind we may easilier accept that when fitting with the electron transverse temperature as the only free parameter to measurements of the cooling time versus the electron current, we find that it is necessary to increase the electron temperature with decreasing current in order to match the cooling times found in measurements. This behavior could, as discussed be due to the lack of intra-beam scattering in the ion beam in the simulations, but may also be due to misalignments which become more influential with larger space-charge effects in the electron beam, and may have increased the cooling efficiency at higher currents.

One observation is however of importance here. It seems that we in general can reproduce the measurements with the old electron cooler setup (1.5 m solenoid), whereas with more or less all of the measurements done with the new setup the reproduction is unsatisfying. This does suggest that there may have been some problems with the new cooler, as even measurements with the same lattice does not reproduce with the long cooler. This is however only speculations, but it seems likely that the new setup, which only existed for a short time, and therefore did not benefit from the same amount of operational experience as the old, may have been in a less well defined state than the old.

Thus we seem to have a simulation routine which to a large extent can predict most of the

observed behavior, and also gives reasonable estimates of cooling times. But it should be handled with care, in the sense that a reasonable amount of the parameter space should be investigated for each setting in order to make believable predictions.

Chapter IV

Electron cooling in the AD

In this chapter we use the program BETACOOL which we have studied in the previous chapters to calculated cooling down times in the Antiproton Decelerator (AD).

4.1 The Antiproton Decelerator (AD)

In the Anti-proton Decelerator (AD) the beam is to be electron cooled at two different energies to compensate the adiabatic blowup during acceleration. For this purpose a flat-top is foreseen at a momentum of 0.3 GeV/c and one at 0.1 GeV/c - from which the beam is also extracted into the experiments.

Table 4.1 shows the parameters for the AD electron cooler (which is the former LEAR electron cooler used for the previously discussed experiments, and modified to adapt it to the requirements of the AD).

With the program BETACOOL we have estimated the cooling time at the two flat-tops as a function of various ring and beam parameters. The time available for cooling and the desired emittances are given in table 4.2 taken from the AD design study [1].

In the following calculations the values from Table 4.2 and Table 4.1 have been used when nothing else has been stated. This means that the initial horizontal emittance and vertical emittance has been assumed identical, and that the calculations have been done for particles with single particle emittances (momentum spreads) equal to the 2σ emittance (4σ momentum spread) of the beam expected in the machine.

4.2 Cooling at 300 MeV/c

Figure 4.1 and Figure 4.2 show the cooling down times in simulations as a function of various initial conditions and electron cooler parameters respectively. The cooling down time is given as the time it takes to change the initial emittance of 33 π mm mrad to the desired final emittance of 2 π mm mrad.

In Figure 4.1 we observe that there is a relatively large asymmetry in the cooling down times with respect to zero momentum offset. Now in practice the offset will be optimized to give the

Parameter	Value @ 0.3 GeV/c	Value @ 0.1 GeV/c
Electron beam radius	2.5 cm	2.5 cm
Electron current (I_e)	2.5 A	0.3 A
Beam kinetic energy	46.8 MeV	5.3 MeV
Electron kinetic energy	25.5 keV	2.89 keV
Electron transverse temperature	0.1 eV	0.1 eV
Electron longitudinal temperature	$2{\cdot}10^{-4}$ eV	$2{\cdot}10^{-4}$ eV
Cooler length l_{cool}	1.5 m	1.5 m
Δv/v at e-beam edge	$4{\cdot}10^{-4}$	$1.1{\cdot}10^{-2}$
Horizontal beta function at cooler	8.6 m	8.6 m
Vertical beta function at cooler	4 m	4 m
Dispersion at cooler	0.15 m	0.15 m
Horizontal Tune	5.39	5.39
Vertical Tune	5.37	5.37
Solenoidal Field	500 Gauss	500 Gauss

Table 4.1: Relevant parameters of the AD electron cooler and lattice. The circumference of the AD is 182.4 m. Cooler-data are optimistic versions of data taken from [12] and [13].

p	ϵ_i	ϵ_f	$\sigma_{h,i}^{ecool}$	$\sigma_{h,f}^{ecool}$	$\Delta p/p_i$	$\Delta p/p_f$	t
[GeV/c]	[π mm mrad]		[mm]		[%]		[s]
0.3	33	2	8.1	2.0	0.2	0.1	6
0.1	6	1	3.5	1.4	0.3	0.01	1

Table 4.2: Transverse emittances (2σ) and momentum spread (4σ) before (i) and after (f) electron cooling, and times available for cooling (see Ref. [1]). The horizontal beam sizes at the electron cooler corresponding to the emittances are also shown. Only adiabatic increase due to deceleration is considered.

beam cooling, and as $\Delta p/p = +0.2\%$ is the 4σ momentum spread the cooling down times for +0.2% alone are the predictions we can extract from the simulation. For completeness (and to monitor for variations) we have however included the -0.2% results in all presentations.

The dependence on the initial vertical emittance (for which there is no prediction) is as in the earlier simulations. The total change in the cooling time for a reduction of the initial vertical emittance to zero is approx. -40%. In order to get the worst case estimates the initial vertical emittance in the simulations have been kept at 33 π mm mrad unless otherwise stated.

The dependence on the transverse temperature is weaker than usually observed, which is a desirable feature, as this means less critical setup.

There seems to be almost no variation with dispersion in the cooling section, one observes even a slight increase in the cooling time with increasing dispersion. This is not so surprising if we calculate the cross over point between cooling and heating as a function of dispersion. If e.g. the dispersion is assumed to be 5 m the cross over point is $\Delta x_0 = 2.3$ cm, which is larger than the

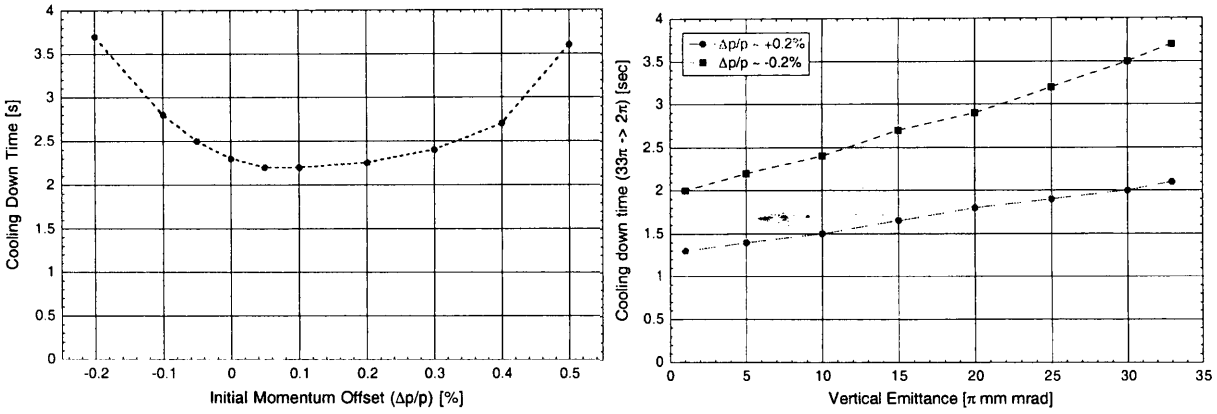

Figure 4.1: Cooling down times from simulations with varying initial conditions for the particle to be cooled. I_e = 2.5 A, $T_{\perp}^{ebeam}$ = 100 meV. Left: Various initial momentum offsets. Right: Various initial vertical emittances (thus in these cases the cooling down time is defined by the change in the horizontal emittance from 33π to 2π).

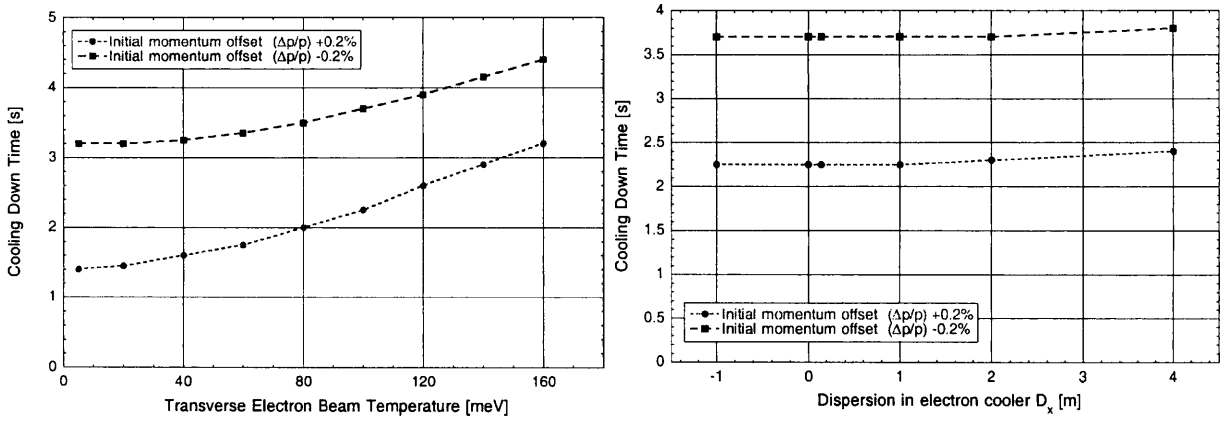

Figure 4.2: Cooling down times from simulations with varying electron cooler settings. Left: Various transverse electron beam temperatures. Right: Changing dispersion in the electron cooler.

beam size (of $\sigma \sim 7$ mm). Thus this simple estimate tells us that the dependence on dispersion should be weak. The cross over point as a function of dispersion for the two AD low momentum flat tops is shown in Figure 4.4.

Generally all the simulations resulted in cooling down times at 300 MeV/c of less than 6 seconds which is the time slot foreseen in the AD cycle. A rough estimate of the e-folding time (of amplitudes) can be found by the following expression :

$$\tau_c = \frac{t_{x16.5}}{\ln\sqrt{16.5}} = 0.71 \cdot t_{x16.5} \tag{4.1}$$

where $t_{x16.5}$ is the cooling down time from 33π mm mrad to 2π mm mrad (a factor 16.5 in emittance (2σ) means square root of 16.5 in amplitude). The cooling down times from the simulations and thus the corresponding e-folding times are are of order 2-3 seconds.

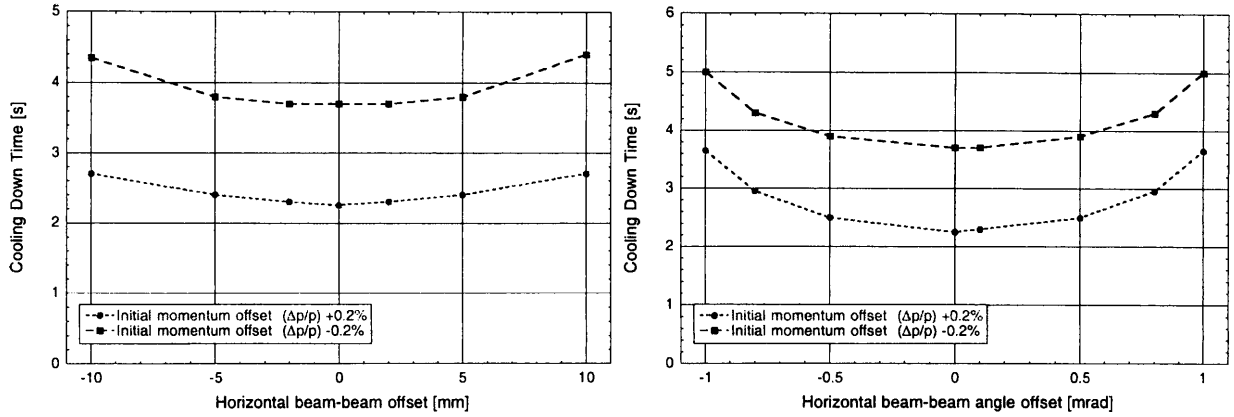

Figure 4.3: Cooling down times from simulations with varying electron cooler settings. Left: Horizontal offset between electron and antiproton beam. Right: Horizontal angle between electron and antiproton beam.

These times should be compared to the heating rates from intra-beam scattering and multiple scattering on the rest gas.

Using the program INTRABTC the transverse heating due to intra-beam scattering can be found as a function of the transverse emittance. The results of such calculations are shown in figure 4.5.

Figure 4.5 shows the relaxation times due to intra-beam scattering in the circulating proton beam in the AD. Even though it is probably not quite the case the relation of the two emittances has been kept constant for the calculations - and as we can see the time scale of intra-beam scattering effects are many orders of magnitude larger than the time scale of the electron cooling. We can thus ignore intra-beam scattering in these beams at 300 MeV/c.

The heating due to multiple scattering on the rest gas, can be found using the expressions discussed in Ref. [4]. With the standard AC vacuum composition and a Nitrogen equivalent gauge pressure of $5 \cdot 10^{-10}$ Torr (which is measured pressure in the AD in Dec. 1998) we find a heating time constants (e-folding) between 300 s and 5000 s for emittances from 2π mm mrad to 33π mm mrad. These times are much larger than the cooling times and therefore negligible in this context.

In Ref. [4] we calculated an equilibrium emittance arising from the equilibrium between an electron cooling rate (e-folding) and the blow up due to multiple scattering. If we use the same equations, and a cooling time of 3 seconds, we get an equilibrium of 0.04 π mm mrad. This is more than an order of magnitude below the design specifications. Thus at 300 MeV/c there seems to be no cause for worry.

4.3 Cooling at 100 MeV/c

At 100 MeV/c we expect electron cooling to be faster, as the efficiency increases with decreasing β, therefore only 1 second has been reserved for electron cooling at this momentum. However, the heating due to multiple scattering is increased a lot, another reason to work fast at 100 MeV/c.

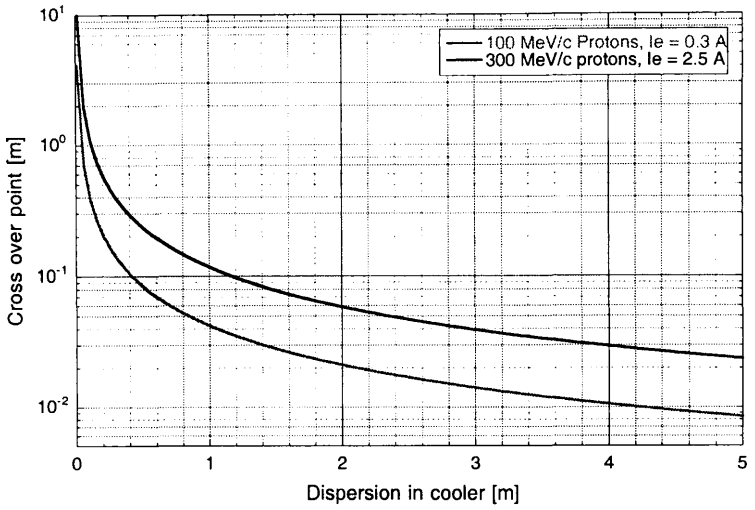

Figure 4.4: Cross over point as a function of dispersion in the AD.

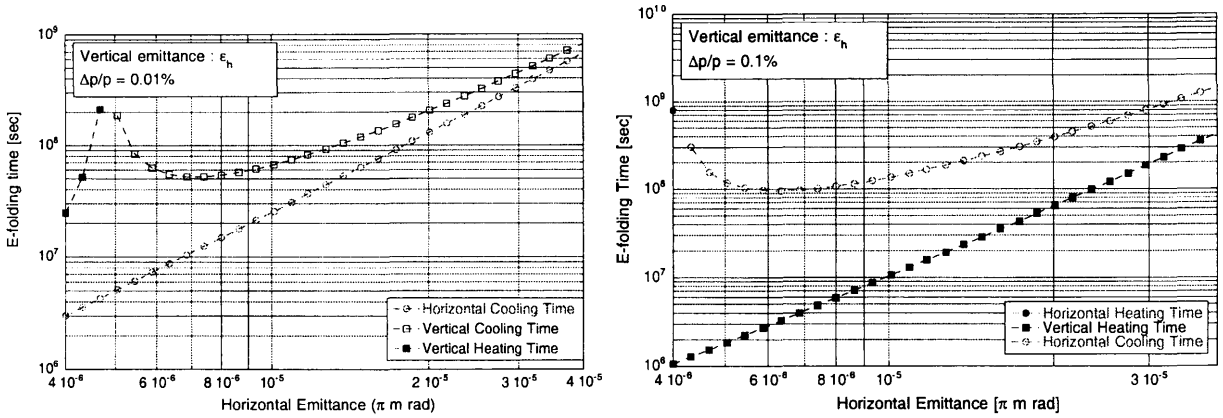

Figure 4.5: Transverse heating and cooling times (shown with the same sign in order to use log-scale) in an AD antiproton beam of 10^7 particles with a momentum of 300 MeV/c calculated using INTRABTC.

Using the program BETACOOL we have simulated the cooling, now at 100 MeV/c.

Figure 4.6 shows the simulated cooling down times ($6\pi \rightarrow 1\pi$) for various initial conditions of the circulating anti-proton beam. As in the 300 MeV/c case the times are usually slightly shorter than the time slot reserved.

Figure 4.7 shows how the cooling down time varies as a function of some parameters of the electron cooler. As we can see 0.3A is about the optimum suggested by the simulation for the chosen setting (for the calculations the worst case was chosen, with initial emittances of 6π mm mrad). However the dependence on the electron beam's transverse temperature is much stronger, and only a moderate increase compared to the "design" temperature may cause the cooling to be too slow. This means that alignment may be very critical at this energy.

As before we should also look at how the cooling time varies with dispersion in the cooler. The theoretical cross over point between heating and cooling is Δx_0 = 1.5cm for D = 5.0m, thus

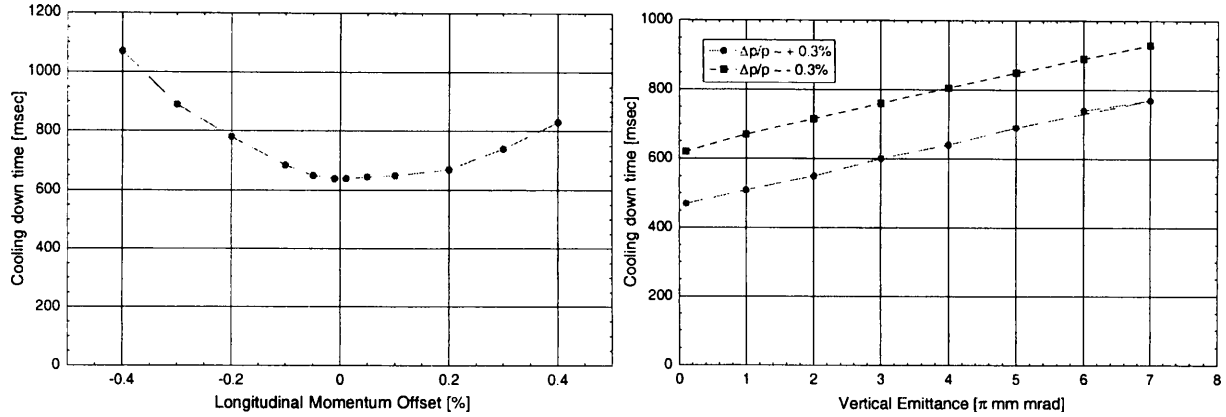

Figure 4.6: Cooling down times from simulations with varying initial conditions. I_e = 0.3 A, $T_{\perp}^{ebeam}$ = 100 meV. Left: Various initial momentum offsets. Right: Various initial vertical emittances.

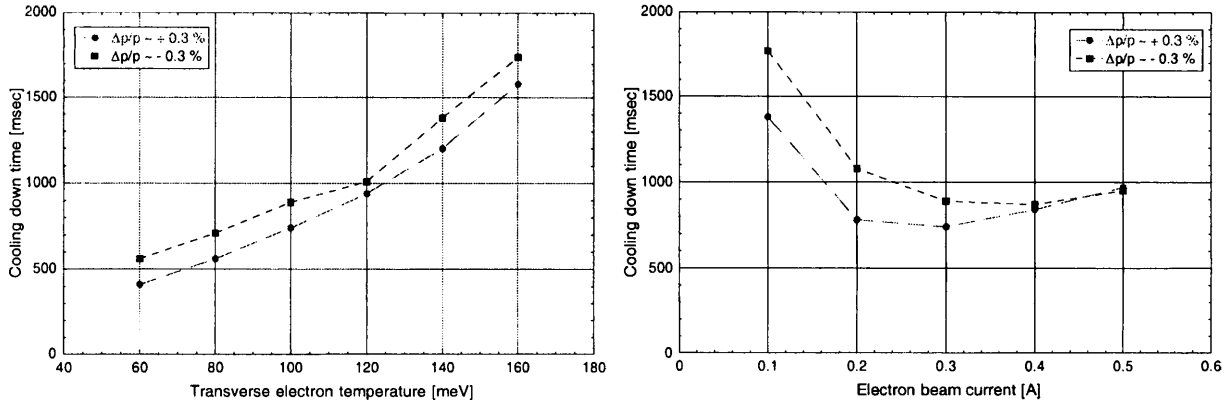

Figure 4.7: Cooling down times from simulations with varying e-beam parameters. Left: Various electron beam temperatures. Right: Various electron beam currents.

as for 300 MeV/c we expect only weak dependence. The dependence on dispersion shown in Figure 4.8 is indeed weak.

Again we need to consider the heating mechanisms which are not included in the simulation, in order to compare the magnitude of these with the electron cooling times. For comparison we can find the e-folding cooling time of electron cooling from the cooling down times as

$$\tau_c = \frac{t_{x6}}{\ln\sqrt{6}} = 1.12 \cdot t_{x6} \tag{4.2}$$

which with a typical cooling down time of $\sim$ 0.7 seconds gives an e-folding time of $\sim$ 0.8 seconds.

The heating time due to scattering on the rest gas is found to be between 6 seconds and 34 seconds for a beam of 1 π mm mrad and 6 π mm mrad respectively. These times are comparable to (but longer than) the cooling time of electron cooling (of $\sim$ 1 second) and the equilibrium emittance which can be estimated from this heating rate is 0.3 π mm mrad, below the design specifications.

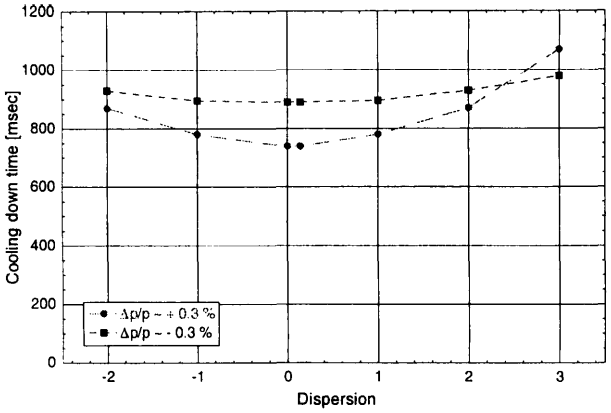

Figure 4.8: Cooling down times from simulations with varying electron cooler settings. Left: Varying dispersion in the cooler.

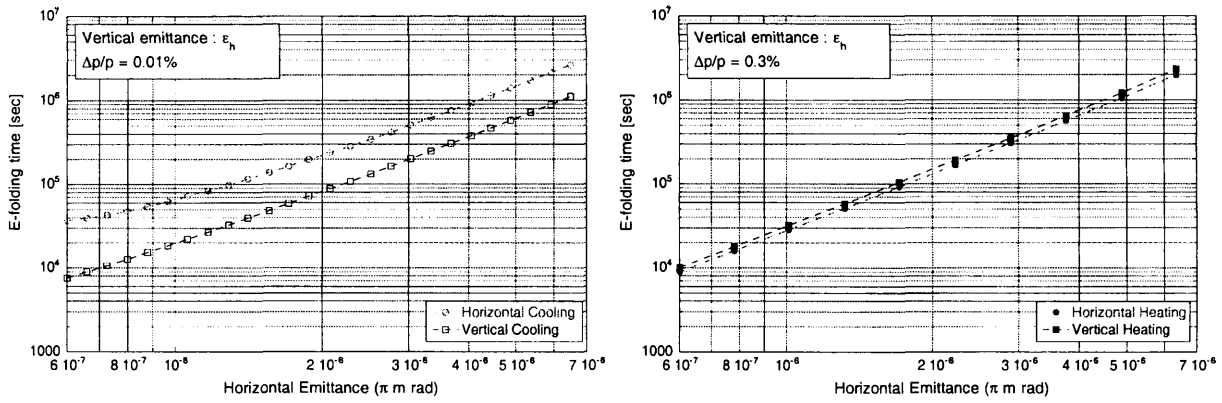

Figure 4.9: Transverse heating and cooling times (shown with the same sign in order to use log-scale) in an AD proton beam of 10^7 particles with a momentum of 100 MeV/c calculated using INTRABTC. The vertical emittance was the same as the hoirzontal for the calculations.

Figure 4.9 shows the heating and cooling times due to intra-beam scattering for 10^7 particles as calculated by INTRABTC. For the calculations the horizontal and the vertical emittance were again kept the same, and the figure shows results for the initial and final momentum spread. We observe that all times are several orders of magnitude larger than the electron cooling, thus intra-beam scattering should not affect our conclusions.

In conclusion the greatest worry at 100 MeV/c as expected is the vacuum. But with careful alignment the simulations and calculations indicate the cooling is strong enough so that with design goals pressure of $3 \cdot 10^{-10}$ torr the desired equilibrium emittance should be reachable.

4.4 Conclusions

We have, using BETACOOL, studied electron cooling in the Antiproton Decelerator (AD). Electron cooling at two different antiproton momenta are needed for the machine, at 300 MeV/c and

100 MeV/c. The simulations show cooling down times for the 300 MeV/c beam which are well within the design specifications, and for the 100 MeV/c they are very close to the design specifications. A series of simulations with various initial parameters, showed that these results are quite stable to the initial conditions, and therefore with the experience gained in the previous chapters we expect them to give a good estimate af the expected performance in experiments. Thus we have found that the design specifications of the AD should be possible to obtain, however at 100 MeV/c care needs to be taken with the adjustment, as the cooling time at this momentum is very close to the upper limit of the specifications.

Chapter V

Conclusions

Electron cooling has been investigated with focus on the electron cooling simulation code BETACOOL. In order to obtain an understanding of the mechanisms important for electron cooling a series of analytical estimates were first made. The suggestions from these estimates were generally in agreement with the simulations, which was also to be expected as the code to a large extent is using similar analytical equations for the calculations.

These results were compared with experimental results from the LEAR machine at CERN. The experimental results consisted of two sets of measurements, the first set with Lead ions and the second with electron cooling of protons. Furthermore two different cooler setups were used with two different interactions lengths, and also different positions in the storage ring. The simulations showed good agreement with the experiments for the experiments with the short (and old) electron cooler, but some fitting of the electron temperature was needed in order to obtain perfect matching. However, the simulations did not agree quite as well with the results from the new (long) cooler, where large discrepancies between simulations and experiment were observed when the alignment between ion beam and electron beam was changed. However for standard operational values of the cooler and the alignment the agreement was reasonable, however not as good as with the old cooler. No definite explanation for the discrepancies were found, but it is believed possible that some uncontrolled parameters may have entered in the experiments with the new cooler, which, being only operational for one year, did not benefit from the same amount of experience as the old one.

Generally we however found that the agreement was good enough that we have used the simulation code to simulate electron cooling in the Antiproton Decelerator (AD), which is presently being commissioned at CERN. We found that the simulations for the AD were stable to variations in the initial conditions which give confidence in the results. The result of the simulation of electron cooling in the AD is that at a momentum of 300 MeV/c the design goals were easily met, whereas at 100 MeV/c the design goals were just met. Thus the AD should not experience problems in meeting its goals, but some care needs to be taken at a momentum of 100 MeV/c to meet the design emittance of 1 π mm mrad.

References

[1] S. Maury, "Design Study of the Anti-proton Decelerator: AD", CERN/PS 96-43 (AR), (1996)

[2] N. Madsen, in "Beam Evolution in the Antiproton Decelerator (AD) under the Influence of Residual Gas and Intra Beam Scattering", CERN PS/DI 99-06.

[3] N. Madsen, in "Beam deterioration by multiple scattering on rest gas", AD-Note 97-12, CERN, 1997.

[4] N. Madsen, O. Gröbner, S. Maury and D. Möhl, in "Beam Lifetime in the Antiproton Decelerator (AD)", AD-Note 97-14, CERN, 1997.

[5] A. Lavrentev, I. Meshkov, A. Sidorin and A. Smirnov, *to be published*

[6] J. Bosser, C. Carli, M. Chanel, C. Hill, A. Lombardi, R. Maccaferri, S. Maury, D. Möhl, G. Molinari, S. Rossi, E. Tanke, G. Tranquille, M. Vretenar, *Experimental Investigation of Electron Cooling and Stacking of Lead Ions in a Low Energy Accumulation Ring*, Internal Note, CERN/PS 99-033, Submitted to Part. Accel. (1999).

[7] I.N. Meshkov, Phys. Part. Nucl. **25**, 631 (1994)

[8] N. Madsen, in "Dynamics of laser-cooled ion beams", Ph.D. Thesis, University of Aarhus, Denmark (1998)

[9] G.K. Parks, *Physics of Space Plasmas*, (Addison-Wesley, Redwood), 1991.

[10] R. Giannini and D. Möhl, in "Improvements of intrabeam scattering codes intrab", CERN PS/AR/Note 96-19.

[11] M. Chanel, CERN/PS, Private Communications (1999).

[12] J. Bosser *et al.*, "Status of Electron Cooling Experiments at LEAR", in Proc. Workshop on Electron Cooling and New Cooling Techniques, (World Scientific, Singapore), 7 (1991)

[13] J. Bosser, "Review of recent work on electron cooling at LEAR", in Proc. Workshop on Crystalline Beams and Related Issues, (World Scientific, Singapore), 435 (1996)

Distribution :

B. Allardyce
P. Belochitskii
J. Bosser
C. Carli
F. Caspers
M. Chanel
V. Chohan
G. De Ninno
T. Eriksson
J-Y. Hémery
E.B. Holzer, EP
J-L. Mary
S. Maury
D. Möhl
H. Mulder
E. Mustafin
F. Pedersen
G-G. Rentier
G. Segura Millan, EP
J. Tan, EP
G. Tranquille